university of groningen

faculty of science and engineering

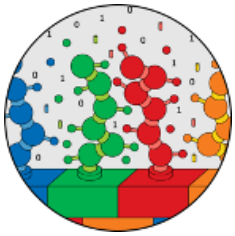

A coarse-grained Molecular Dynamics study of Polyelectrolyte Grafted Nano Particle and Linear Polyelectrolyte solutions.

Wouter Johannes Henri Arends

s3677540

26-06-2024

university of groningen

faculty of science and engineering

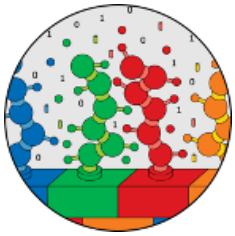

University of Groningen

A coarse-grained Molecular Dynamics study of Polyelectrolyte Grafted Nano Particle and Linear Polyelectrolyte solutions.

Master's Thesis

To fulfill the requirements for the degree of
Master of Science in Chemistry
at the University of Groningen under the supervision of
Dr. D. Maniar (Zernike Institute of Advanced Materials, University of Groningen)
and
Dr. A. Giuntoli (Zernike Institute for Advanced Materials, University of Groningen)
and daily supervision of
Utku Gürel

Wouter Johannes Henri Arends (s3677540)

June 26, 2024

Contents

Abstract

Coarse-grained molecular dynamics simulations show the shape control of polyelectrolyte grafted nanoparticles, PE-GNPs, by adding oppositely charged linear polyelectrolyte, LPE. Over two decades ago, an ultra-soft interaction potential was found for PE-GNPs, hypothesizing exotic phase behavior. Computational limitations restricted systematic simulations of multiple PE-GNP and LPEs. This work builds on the current understanding of a single PE-GNP, investigating the concentration effects introduced by multiple PE-GNP. The combined effects of LPE replacing counterions and multiple PE-GNPs in solution are reported in this thesis. The degree of neutralization, and LPE length are studied in concentration corresponding to the dilute and overlap regime. In the dilute regime, adding LPE leads to a collapse of the PE-GNP, which agrees with the literature. Reaching high neutralization, meaning many LPE and few counterions, dimerization occurs for dilute systems. At high neutralization and above the overlap concentration, all PE-GNP aggregate. The effect of dimerization and complete aggregation completely shifts the behavior of the PE-GNP. It changes from overlap behavior that homogeneously maximizes space occupation to a system that minimizes surface area and undergoes liquid-liquid phase separation. The former has polyelectrolyte arms of the PE-GNP contracting to accommodate one another, and the latter has interpenetrating arms at a concentration below the semidilute regime. These findings are relevant in guiding the post-synthesis modification of the shape and size of PE-GNPs, directing the system towards appropriate model systems for solution properties.

1 Introduction

Polymer research is at the intersection of physics, chemistry, biology, and engineering. The combined effort has progressed humans from the Iron Age to the Age of Plastics. The field describes the synthesis, characterization, understanding, and engineering of materials from atomic to macro scale. Current advancements in polymer synthesis provide controlled ways to make cyclic-, star-, brush-, comb-, block-co-, triblock-co-, and dendritic polymers.[1]–[3] With the many advantages of using traditional petrochemical polymeric materials, such as durability and processability, comes a great price. Plastic waste is piling everywhere, from the Great Pacific Garbage Patch to microplastics in human testicles.[4]–[6] Current innovations steer towards renewable sources to replace petrochemicals, biodegradability, and enhanced properties to minimize plastic usage. Current efforts towards bio-degradable polymers require modifications to be processable as the more resistant petrol-based polymers.[7] A fundamental understanding of the polymers and processing involved is critical to properly finding and utilizing enhanced properties. The newly available polymers drive the research for structure-environment-properties relationships in polymer science.

Macromolecules pose a multiscale challenge, where a single polymer chain ranges from angstrom to multiple nanometers in size.[8], [9] Involving chain conformation, lamellar crystallization, and chain relaxation. Multiple macromolecules increase this towards micrometers, where networks[10], self-assembly, formation of spherulites[11], and viscoelasticity arise.[12] Understanding polymeric materials starts experimentally at the atomic scale; Nuclear Magnetic Resonance, Infra-Red spectroscopy, or High-Pressure Liquid Chromatography characterize a polymer to find the composition, degree of polymerization, and polydispersity indexes. With these techniques, the atomic structure can be determined with high efficiency. Polymeric materials experience a resistance to stress due to the timescales of intrapolymer relaxation and intermolecular reorganization. The dynamics of such systems, polymer coils, are studied in soft matter, relating a material's solid and fluidic behavior. Research focuses on the connection between microscopic structure and macroscopic properties of colloids, liquid crystals, and, concerning this work, polymers. The relevant systems are studied by means of scattering experiments, light, neutron or X-ray, electron microscopy, and rheology.[13] These methods probe the size, orientation, and dynamics in an indirect manner. A more direct understanding of how particles move is required to understand the mechanisms involved further. This has been achieved with Molecular Dynamics (MD).

A class of particles currently being researched is the polyelectrolyte grafted nanoparticles(PE-GNP), consisting of a core area, rigid, frozen, or flexible, and charged polymers protruding from the core. The effective potential between these particles was found to be ultra-soft.[14] Such potentials are predicted to have a rich phase behavior, including re-entrant melting and exotic crystal phases. Typical polymer chains are tenuous, making them soft and not elastic; hard spheres are dense, making them hard and infinitely elastic.[15], [16] The PE-GNP, while remaining tenuous, displays soft and elastic behavior, forming glasses and caging at low-volume fractions compared to the 0.58 volume fraction of hard spheres.[17], [18] Some applications are in drug delivery[19], [20] with large size and charge dependencies or adsorption and surface spreading antifouling coatings.[21], [22] Or polyionic liquids can be used as nanoreactors.[23] Another application is enhanced oil recovery, where viscosity is reduced.[24] Responsive systems with shape and viscosity control are vital for these applications. Temporary shape control through solvent quality[25], salt concentration[26], electric field manipulations [27], and other methods have recently been gaining traction to fulfill the need for better properties in barriers, yarns, drug delivery, and the ability to process non-conventional polymers on a large scale.

A different approach to control the size of PE-GNPs is to add multivalent species, such as multivalent salt or linear polyelectrolyte (LPE), instead of monovalent counterions. The theory of PE-GNPs with monovalent counterions is well understood. Systems with multiple PE-GNPs in solution are described in theory, simulations, and experiments. These studies have documented the effects of concentration, showing a retraction of arms before interdigitation.[28], [29] The behavior for different salt concentrations is apparent in these works, intricating the mechanisms involved. This work will consider the addition of LPE to modify the PE-GNP reversibly after synthesis. Previous work theory and simulations have been done for single-particle systems with star polymer-linear polymer interactions[30], interactions between spherical polymer brushes(SPB) and LPE[31], and SPB with multivalent salt[32], as well as a model for a non-viral gene factor.[33] These single-molecule systems are dilute and fixed in space. Experimental efforts use multiple particles as they are hard to isolate.[34]. This work combines these two lines of research: concentration effects and LPE complexation effects.

Similar models are being studied, focusing on the assembly of oppositely charged PE-GNP.[35], [36] These show well-defined supramolecular organizations that depend on interaction parameters like more classical block-copolymer phase-separation. The key difference is that the parameters for PE-GNP assemblies are temperature and ionic strength instead of temperature and the interaction parameter, χ. The classic example of block copolymers is polymer-polymer phase separation, and the PE-GNPs undergo liquid-liquid phase separation. Also, other polymeric substances and architectures, such as dendrimer conformations, are under investigation.[37]–[39] Self-assembling block-co-polymers are also studied in Non-equilibrium Dynamics.[40] The assemblies of planar polymer brushes and charged surfactants were studied, showing structural patterning.[41] The patterns depend on the charge ratio, a measure of how many brush-neutralizing particles are present. In this work, this is referred to as the degree of neutralization. Oppositely charged diblock copolymers can be added to model the zipper brush.[42] More closely related to the frozen core micelles is a similar model that does not make the assumption of the core being a single particle.[43] Perhaps most reminiscent of the current work is the theory [44] and simulations [45] efforts towards understanding hybrid colloid-polyelectrolyte conservation. These works use colloids as a model system for globular protein, solid nanoparticles, or spherical micelles. The common ground between these works becomes more apparent with the considerations of when a branched polymer becomes a particle.[46] This is with five or more arms. The key difference is that there is space for linear polyelectrolytes to penetrate the star, whereas the colloids do not have this space. This is also shown for SPBs, where one sees lateral and radial surface patterns for respectively low and high grafting density. [47]The main contributions to the coacervate's internal structure are the adsorption strength of the polyelectrolytes and the ratio between the polymer shell and core radius.

These MD simulations are coarse-grained molecular dynamics (CG-MD), as atomic and monomeric precision is forsaken to obtain reasonable timescales and statistics with the current resources. The shaving away of details is depicted in figure 1.1. Quantum effects are not captured in all-atomistic simulations (AA). The characteristics of individual atoms or monomers are left out in CG-MD. Molecular details are lost when transitioning to continuum simulations at the mesoscale or macroscale. Over the last 15 years, these resources have upgraded and allowed for more detailed simulations on large molecules, like polymers and proteins, longer timescales, improving access to glassy dynamics, and more particles, allowing investigation of phase behavior and properties in solution and melt. How the potential energy landscape is smoothened with coarse-graining in figure 1.2. Different approaches

are static mapping, dynamic, and reverse mapping.[48] With coarse-graining, one chooses quantitative trends and moves away from qualitative predictions. However, experimental data can be used as input, and the simulations can be used as verification. To further the understanding of systems multiscale modeling approaches to go from atomistic or quantum scale to macroscopic properties, with DFT, AA, CG-MD, and mapping to larger models, such as the tube model[12] or employing interaction potentials.[49]

Previous unpublished work of this research group developed a coarse-grained PE-GNP model[18] for verifying experimental systems, such as a star-like block-copolymer assembly aggregating to kinetically frozen core micelle.[2] The overlap concentration was related to a vitrified state, showing a liquid-to-solid transition. The scaled-down model[50] was investigated for grafting density, degree of polymerizations of the arms, and concentration effects related to shape control. The entropic penalty for linear chains condensation is much less than counterions and will be osmotically inactive, preventing counterions from being active in the swelling of the PE-GNP.

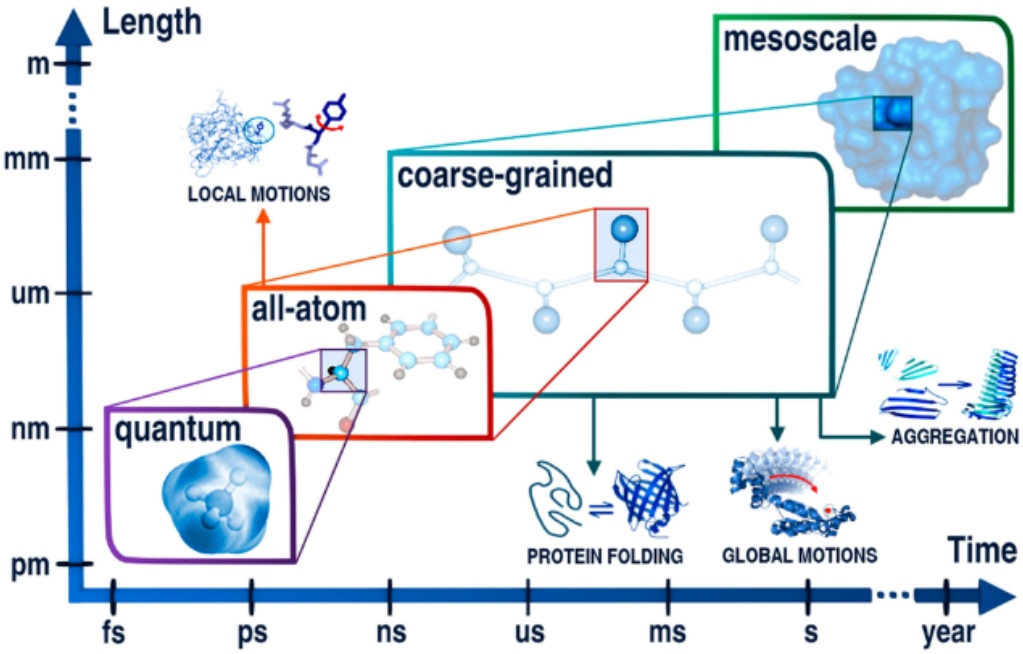

Figure 1.1: Schematic that displays the length scale as a function of the time, that characteristic dynamics of these times and lengths. The schematic shows how one leaves details away from quantum calculations, such as density functional theory (DFT) or Hartree-Fock (HF), towards all atomistic classical dynamics that can be grouped in coarse-graining as four beads per amino acid, going further to 1 bead per amino acid or a Kuhn segment. Coarse graining further, one will end up towards dissipative particle dynamics or continuum simulations at the mesoscale.[51]

In this work, the scaled-down model is further explored by systematically varying the number of LPEs, ranging from no neutralization to complete neutralization, and the length of the LPE, in the range of a dimer to polymers longer than the PE-GNP arms. This is performed in the dilute and overlap regime. An ensemble of 64 PE-GNP will be simulated using CG-MD simulations employing a bead spring model with implicit solvent. The simulations are limited to no additional salt to increase simplicity and decrease computational costs. Simulations were run with the Large-scale

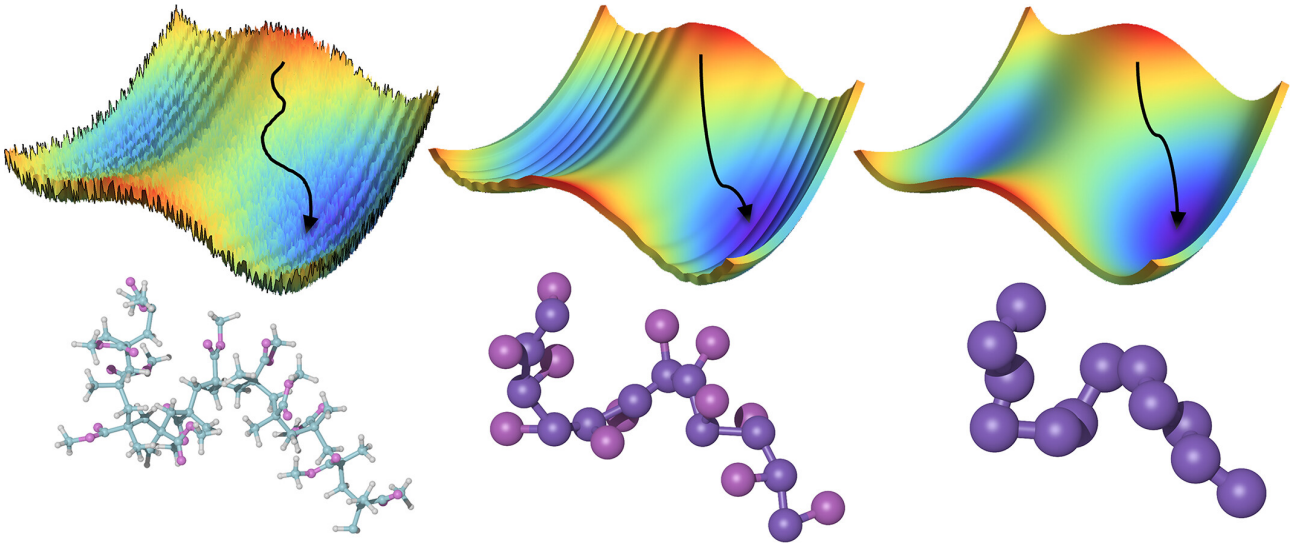

Figure 1.2: Graphical representation of what occurs with coarse-graining to the structure of molecules and the free energy landscape.[52] Starting on the bottom left is an all-atomistic representation, and going to the right, it coarse-grains further. The corresponding free-energy landscapes are shown from the top left to the top right, and one can appreciate how the global minimum becomes more available.

Atomic/Molecular Massively Parallel Simulator, LAMMPS.[53] The aim is to uncover the structural relationship with the addition of LPE and multiple PE-GNPs interacting. The gyration tensor, radial distribution function, RDF, and mean square displacement, MSD, are used to characterize this behavior. These give insight into the shape, size movement, and relative position. The system's dilute behavior was validated with single PE-GNP simulations.[31]–[33] The multiple PE-GNP investigation elucidated the hypothesis that aggregation of PE-GNPs would occur at complete neutralization and displays the concentration and LPE length dependence.

2 Theory

To understand the MD simulations and what information stems from them, the following chapter will explain the key concepts that form the background of the research project. These are Polymers and soft matter, Poly Electrolyte-Grafted Nano Particles (GNP), and complex coacervation.

2.1 Polymers and soft matter

Polymers are classified as soft matter and, therefore, deformable and influenced by their environment. Extrapolating from an inherent quality, such as the molecular weight towards the polymer coil size in solution, is not as straightforward as it would be for a hard sphere. The Zimm model[54], [55], assuming solvent being dragged with the polymer within its pervaded volume, in combination with the mean-field model by Flory [56], [57] The radius of gyration, R_g, and molecular weight, M_w, are related to one another with the exponent ν. The exponent for linear polymer chains used in equation 2.1 $\nu = 0.6$ in dilute good solvent conditions. Increasing the concentration of polymers quickly complicates the situation.[58], [59]

$$R_g \approx M_w^{\nu} \tag{2.1}$$

Relating the inherent M_w to something that describes the size of the coil that can be further related to macroscopic properties brings predictive power and planning for specific applications. Further challenges arise when introducing more relevant chemical interactions and varying the architecture. For neutral and charged star polymers, scaling depends on the degree of polymerization and the number of arms. Daoud and Cotton found scaling laws describing this behavior.[60] For the number of arms, degree of neutralization, Kuhn length, and excluded volume selected for this system, the following scaling would apply $R = M^{3/5}v^{1/5}F^{1/5}b$. [50], [60]. Scaling complicates star polyelectrolytes further, with the condensation of counterions becoming an important parameter. Translating the M_w towards R_g is relevant because this relation gives insight into the more relevant coil size or star size, R, and viscosity, η. R_g and R are related for this system in Appendix A. The viscosity of neutral polymer melts in the unentangled regime $\eta_0 \approx N^{1.0\pm0.1}$, where N is the degree of polymerization of a linear polymer.[25] For entangled polymers, it scales as follows, $\eta_0 \approx N^{3.4}$. For soft colloidal suspensions, a nonlinear rheological response is observed.[61] The material displays both glassy responses, resisting sheer at high concentrations and at low concentrations where there is little resistance.

The ratio between the radius of gyration and the contour length l_c indicates how extended a polymer chain is. This indicates the solvent quality of the system. A low ratio suggests bad solvent conditions and a high ratio indicates good solvent conditions. How polymers mix considers the solvent quality and the interaction between polymers. Flory's theorem describes mixing and balancing the favorable enthalpic interactions and unfavorable entropic contributions from constrained chains.[57] Flory theorem: polymers in the melt behave similarly to ideal chains without excluded volume. This does not generally apply to polymers with non-trivial topology. The Rouse model describes polymers as a series of connected beads without hydrodynamic interactions. It is not ideal for dilute systems, but it proposes that viscosity is proportional to molecular weight. The Zimm model builds further upon the Rouse model and includes hydrodynamic interactions. This proposes correct values for the intrinsic viscosity. These models follow the Fox-Flory equation, leading to the Mark Houwink equation.[25] Both are given below:

$$[\eta] = \Phi\frac{R^3}{M_w} = KM_w^a \tag{2.2}$$

R being the coil size $R \approx b\sqrt{N}$ square root of monomers with size b (number of beads of size b), $\Phi = 0.425 N_a v$ and $a = 3\nu - 1$. In θ solvent a = 0.5 and good solvent $a = \cong 0.76$, entangled star polymers mainly rely on the number of entanglements per arm for their viscosity. It is independent of the number of arms. The mode of relaxation is the retraction of the arms. The introduction of LPE will limit this. Polymers are not limited to dilute solutions or melts. They form arrested states, networks, and gels, each influencing the viscosity and dynamic properties in their way.

2.2 PE-GNPs

Polyelectrolyte grafted nano-particles, PE-GNP, is not a common term; it will be defined, and some characteristics will be explained in detail. A nano-scale particle, monomers, aggregates, or typical metal or polymer particles constitute the core. From this core, polymer arms protrude. These polymers are charged species and called polyelectrolytes. Classes that fall under this term are: Star-polymers [28], [29], charged frozen core micelles[2], [18], spherical polymer brush[13], [34]. For star polyelectrolytes,[28] and polyelectrolyte brushes[62] theory has been well defined, with scaling laws for different regimes in the presence of counterions and salt. Allowing simulations to test these theories and use them to build models. The same will be done in this thesis.

Polymers are typically depicted as linear, but unintentional branching occurs during production. This has evolved into intentional branching. A single central branching point is a star polymer; if it branches more in the subsequent linear chains, it becomes a dendrimer. If it has multiple branching points on a linear point, it can be a brush polymer (dense) or a comb polymer (sparse), depending on the grafting density. A polymer brush is a surface grafted with linear polymer chains, where the surface is flat or curved for a spherical polymer brush.

2.2.1 Star polyelectrolytes

Star polymers are considered to behave as typical linear polymers with five or fewer arms. With more arms, behavior tends to be more particle-like.[46] This work will focus more on particle-like polyelectrolyte stars. The behavior of polyelectrolytes can be subdivided into three concentration-dependent regimes.[28] Two classical regimes are dilute and semidilute. The third regime is specific for polyelectrolytes: overlap. These transition into one another with increasing concentration from dilute to overlap to semidilute. In the dilute regimes, polymer chains are far apart and barely interact with other polymer chains. The semidilute regime is characterized by polymers interacting and mixing and, for stars, interpenetration. The overlap regime also has interaction between stars. However, there is no mixing or interpenetration. Instead, to accommodate the space, the arms of a star retract. Once this is no longer possible, arms will interpenetrate, which is considered a semidilute regime. These regimes are characterized by the distance between the center of mass of the star, which is defined as

$$R_{cm} \approx b \left(\frac{fM}{cb^3} \right)^{1/3} \tag{2.3}$$

The f is the functionality of the star, b the Kuhn length, M the number of monomers in a PE-GNP arm with length b, and c the concentration. If the distance between neighboring stars is much larger than the radius of a star, it is defined as the dilute regime. In the overlap regime, the R_{cm} is on the order of the radius of a star. From this follows the overlap concentration

$$c* \approx \frac{fM}{R^3} \tag{2.4}$$

when R_{cm} becomes smaller behavior will be semidilute. The concentrations at which this happens differ depending on the dominant effects. Shusharina and Rubinstein have provided a full description of the scaling of these systems based on the number of arms and concentration, with and without salt.[28] A graphical representation is presented in figure 2.1. To understand this, the condition for ion condensation needs to be clarified

$$u^2 a > 1, \tag{2.5}$$

where u is the ratio between the Bjerrum length and the Kuhn length, $u \equiv l_b/b$. The Bjerrum length is the length at which Coulombic forces are equal to the thermal forces. a stands for the fraction of monomers or beads that are charged. In the case of equation 2.5 indicates counterion condensation, contrarily below 1, counterions do not condensate. The Manning condition for condensations states that the charge per Bjerrum length should be smaller than the linear charge density[63], as is described in equation 2.5. To better understand what this means, the Wiegner-Seitz cell is introduced.[64] This cell has three areas: surrounding the core and proximal to the arms, V_1, in the interarm space, V_2 and outside the PE-GNP, V_3. A counterion is osmotically active when it has degrees of freedom, such as translational. In V_1, counterions are condensated and lose most degrees of freedom. There is movement along the chain, leading to some osmotic activity.[34] The correlation is stronger for multivalent counterions or polyions, and osmotic activity is negligible. In V_2, the counterion is non-condensated and osmotically active. When the counterion is outside the star in V_3, it is not osmotically active in expanding the PE-GNP. This work treats condensed and non-condensed counterions as $u^2 a = 1$, with l_b, b, and a set to unity.

In the case of $u^2 a > 1$, counterions are condensated. This means no dilute polyelectrolyte regime exists. This regime is characterized by ions moving freely through the solution. This is rooted in the entropic penalty for confinement being larger than the potential gains from electrostatic interactions. The osmotic and quasineutral regimes are present when ions condensate. Extended arms that are pushing against each other characterize these regimes. The origins are counterions that are osmotically active inside the star and a high segment density in the PE-GNP, forcing extension similar to a neutral dense system. Translating this towards LPE, the entropic loss caused by confinement gets smaller with the increasing size of the LPE, as many of the degrees have been restricted by binding. This means that at $u^2 a = 1$, the LPE will condense, and a significant part of counterions are not condensed, either osmotically active or in solution. Figure 2.1 (a) becomes applicable for LPE and Figure 2.1 (b) for counterions.

In the osmotic regime, thermal energy is smaller than the Coulombic interactions, and counterions are confined in the star either way. The size of the star is independent of the number of arms. More arms will eventually lead to the quasineutral regime where segment density is so high that this dominates over short-range electrostatics. Scaling for these different relevant regimes are as follows: for the dilute osmotic regime scales like:

$$R_{OS} \approx bMa^{1/2}, \tag{2.6}$$

This is both for condensated and non-condensated counterions. For $c > c*$, there are multiple regimes of interest where different effects dominate in controlling the shape. In the overlap regime, this is long-range electrostatic repulsion between arms; this can only occur without counterion condensation. In the electrostatic and quasineutral overlap regimes, short-range interactions dominate, respectively,

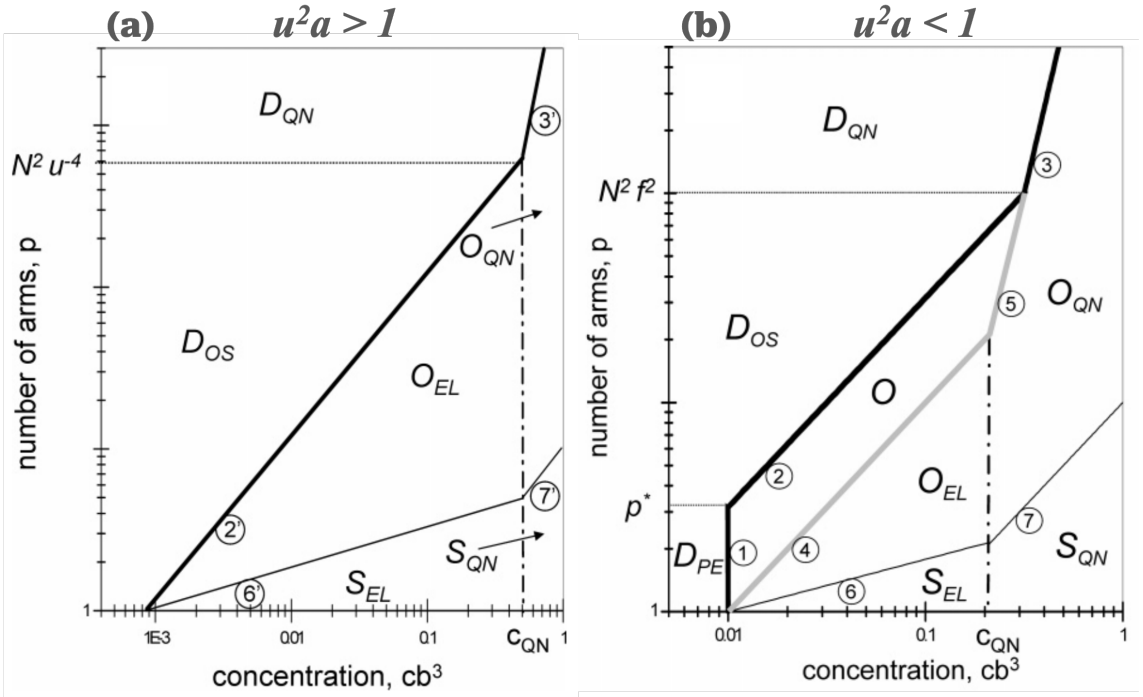

Figure 2.1: Figure adapted from [28], polyelectrolyte star solution regimes as a function of arms, p, and the Kuhn segment concentration cb^3. The limit in the dilute regime number of arms is signified by the number of Kuhn monomers, N, the ratio l_b/b, u, and the charge fraction, f. In this work, the charge fraction is designated with a, as the text mentions. The relevant regimes are explained in the text. The circled numbers signify the crossovers. The relevant ones are $2, 2'$, and the overlap concentrations $c*$.

electrostatically and sterically. Despite different dominant effects, the scaling is the same

$$R_O \approx \left(\frac{fM}{c}\right)^{1/3} \tag{2.7}$$

2.2.2 Spherical polyelectrolyte brushes

The stretched nature of the grafted polymer chains characterizes polyelectrolyte brushes. These polymer chains are smaller than the radius of the particle or surface on which they are grafted. A homogeneous segment density over the brush's height for a conventional brush. In this work, spherical polyelectrolyte brushes, SPBs, are characterized by the same stretched state but an inhomogeneous segment density and a curved surface. The density decreases going radially outward. The presence of multivalent salt or polymeric ions has been studied for polyelectrolyte brushes.[65] For SPBs, this has been studied by means of anomalous small angle X-ray scattering (ASAXS) and small angle neutron scattering (SANS).[13], [66] For single SPBs, CG-MD has been performed.[31], [32]. Osmotic coefficients were experimentally determined.[67] The effective interactions between SPBs were studied, and the PE-star theory previously discussed was extended to the SPB.[14] This produced the predictive model for the osmotic coefficient

$$\Phi = \frac{Q*}{Q_{bare}} \tag{2.8}$$

Where Φ is the osmotic coefficient, $Q*$ is the net charge of the SPB, and the Q_{bare} is the charge of the SPB in the absence of ions. The effective potential found was the shape of an ultrasoft repulsion. Spherical polymer brushes were studied in the context of multivalent salt.[32], [34]

2.3 Complexcoacervation

Complex coacervation refers to associative liquid-liquid phase separation. This type of phase separation occurs when two polymers associate through charged interactions. This results in a polymer-dense phase and a dilute phase, the supernatant. In the case of charged interactions, this can be tuned by salt concentration or pH. The driving forces involved are the enthalpic interaction between salt ions and polymer or polymer-polymer, the entropic penalty for the association of polymers or salt and polymers, and entropic and enthalpic gain for the solvent. The first theory, Voorn-Overbeek's theory, combines Flory-Huggin's theory of mixing and the Debye-Hückel of dilute electrolytes. [26] The enthalpic interactions from the favorable Coulombic interactions will be the same. However, all of the entropic contributions to the system will favor LPE condensation. Arresting a larger molecule is entropically favored over multiple small molecules. The small molecules also do not disrupt the solvent network as much, giving a favorable interaction. This effect is not captured with implicit solvents, unlike other solvent-specific effects. Origins have long been debated, but a clear picture of the interactions involved and the main driving forces are becoming apparent when the interactions of water are fully captured, and this model could provide more insight.[68]–[70] Proteins undergo LLPS based on hydrophobic and Coulomic interactions. Current simulation efforts are focussed on the dominant effects in the coacervation. A more detailed theory on the scaling involved in complex coacervation focuses on further assemblies, such as complex coacervate core micelles and complex coacervate microcapsules.[71], [72] Or on inhomogeneous coacervates.[73] Investigation on different lengths in complexation shows that smaller chains complex faster but are eventually replaced by longer polyions.[74] The replacement was seen to go stepwise and is tailored to the available free charge. Furthermore, they show the shrinkage of the polymer chains upon complexation.

The viscosity of complex coacervates is dominated by the dynamics of single ionic bonds acting as temporary crosslinks between the polyelectrolytes.[75], [76] This is then tunable with salt, decreasing the strength of these crosslinks. Theoretical efforts refer to a "sticky" Rouse model.

3 Methods

In this section, I will discuss how the computer simulations on which this work is based are set up and how the output was analyzed. Molecular dynamics (MD) was employed to emulate how polymeric particles move and interact with their environment and each other. MD simulations can be all atomistic (AA), where every bead represents an atom or coarse-grained, approximating molecules or monomers as an excluded volume with a degree of homogeneity in interaction potentials. Here, we apply a Coarse-grained model based on the same coarse-graining commonly seen in polymer physics, a bead spring model. These respective techniques and fields will be explained to understand the model and how it is coarse-grained.

Molecular dynamics is a widely applied technique using Newtonian physics. Software like GROMACS and LAMMPS [53] are employed to solve the equations of motion for a particle-filled box. This simulation box has a $V = L^3$ volume and several particles inside, n. A typical unit for experimental science is the number of Avogadro $n_a = 6.02214 \cdot 10^{23}$. Currently, systems of such n are not accessible in reasonable timescales. To work around this limitation, periodic boundary conditions have been introduced to simulate bulk materials or solutions.[25] Further reduction in simulation costs can be achieved by implicitly treating the solvent, meaning it is a structureless continuum that causes the solvent-mediated effects on the system. This greatly reduces the number of particles and degrees of freedom. A simulation begins with the following input parameters: initial position $\mathbf{r_i}$, velocity of the particle $d\mathbf{r_i}/dt$ (generated randomly from a velocity seed), Temperature T (stemming from the average kinetic energy), pressure P and interaction potentials between particles.[25] These interaction potentials can be empirical, pair, many-body potentials, or a mix of these examples. Treating the solvent implicitly is performed by adjusting these potentials and shifting or truncating the behavior. This work uses pair potentials, which will be specified in the model's section.

Different dynamics such as Stochastic[33], [77] Brownian[31] and Langevin using the Verlet algorithm [50] or higher order integrators[78] can be applied to include more forces such as drag and overall acceleration or not. Stochastic and Brownian dynamics use stochastic forces and have no net acceleration or drag; Langevin dynamics do to a certain extent. To simulate hydrodynamic behavior properly at larger timescales, possible than AA simulations, one can choose dissipative particle dynamics (DPD).[40], [79] In DPD, multiple solvent molecules are grouped to emulate the hydrodynamic effects properly. This is performed by calibration in post-processing instead of originating from microscopic properties. With the yearly downsizing of chips and other efforts, computational power increases, leading to the ability to probe larger systems. Not only with more computing power but also with coarse-graining, we can achieve larger systems and larger timescales. Coarse graining is the art of taking details away from your molecule while capturing the behavior of interest. This allows us to obtain meaningful qualitative trends. With more multiscale modeling, one can obtain meaningful quantitative data.

The equations that are being solved are called Newton's equations of motion. These arise from the total force on a particle, coming from every other particle. This differs from mean field techniques, and every individual contribution is counted:[25]

$$m_i \frac{d^2\mathbf{r_i}(t)}{dt^2} = - \sum_{\substack{i \neq j \\ 0 \leq i,j \leq n}} \frac{\partial U(\mathbf{r_i} - \mathbf{r_j})}{\partial(\mathbf{r_i} - \mathbf{r_j})} \tag{3.1}$$

These forces sum together as the previously mentioned equations of motion. One integrates numerically over a small timestep to solve these and obtain a trajectory. This can be done by using the Verlet algorithm:

$$\mathbf{r_i}(t+\delta t) = 2\mathbf{r_i}(t) - \mathbf{r_i}(t-\delta t) + (\delta t)^2 \frac{d^2\mathbf{r_i}(t)}{dt^2} \tag{3.2}$$

The Verlet algorithm is used for microcanonical ensembles with a constant number of particles, volume, and total energy (NVE) or constant Temperature (NVT). Both are used and will be discussed in the simulation details. These are Nose-Hoover-style equations of motion that can generate positions and velocities from the aforementioned microcanonical ensembles. More exotic integration methods can be used depending on what is kept constant or when translating AA to CG simulations. [78]

3.1 Model

This research project consists of coarse-grained molecular dynamics (MD) simulations of polyelectrolyte grafted nanoparticles (PE-GNP) and oppositely charged linear polyelectrolytes (LPE). A polyelectrolyte is a charged polymer, either anionic or cationic. These simulations are coarse-grained and are, therefore, in Lennard-Jones units. This increases the characteristic length of the systems and allows for longer timescales than an all-atomistic approach would. The model is based on the Kremer-Grest bead spring model[80]–[82] with a harmonic bond potential[83], truncated-shifted Lennard-Jones (LJ) potential [25], and a Coulombic potential[83]. These will be described in detail here, as well as the other details of the model.

A PE-GNP comprises a core that represents a frozen core from block-co-polymer assemblies, PS nanoparticles, or other grafting points. To this core, polyelectrolytes are grafted to denote the architecture of these polymers f and M is used. f represents the number of arms. M represents the number of beads comprising one arm, the chain length, or the degree of polymerization. The architectural parameters of the PE-GNP are in the low functionality and arm-length limit: f = 16 and M = 30, respectively. The degree of polymerization of the LPE is similarly denoted by N. Counter ions are introduced to ensure charge neutrality when LPE and PE-GNP do not neutralize one another. To model the polymers in good solvent conditions, a shifted and truncated LJ potential [25] is introduced:

$$U_{LJ}(r) = \begin{cases} 4\varepsilon_{LJ}\left[\left(\frac{\sigma_{LJ}}{r+\Delta}\right)^{12} - \left(\frac{\sigma_{LJ}}{r+\Delta}\right)^{6}\right] & \text{for } r \le r_c + \Delta \\ 0 & \text{for } r > r_c + \Delta \end{cases} \tag{3.3}$$

Where ε_{LJ} is defined as the pair strength and set to unity $\varepsilon_{LJ} = 1$ σ_{LJ} is the pair length and the diameter of a bead. These beads represent a Kuhn segment of the polyelectrolytes for both the arms in the GNP and the linear polyelectrolytes. The counterions are also represented by a bead with a diameter of 1 σ_{LJ} and a mass of 1 m_{LJ}. The bead representing the core is the only bead that deviates. It has a diameter of 2 σ_{LJ} and a mass of 8 m_{LJ}. Δ defines the shift of the LJ interaction. These are set separately for each particle type pair. The core-core shift is 1 σ_{LJ}, core monomer(PE-GNP arm and LPE), and core ion shift 0.5 σ_{LJ}. All other interactions are not shifted. Lastly, r_c is the unshifted cutoff distance for the interaction or simply the radius of the bead; these are 2.5 for core-core interactions. For all other interactions, $r_c = 1.12246\sigma_{LJ} \approx 2^{\frac{1}{6}}\sigma_{LJ}$

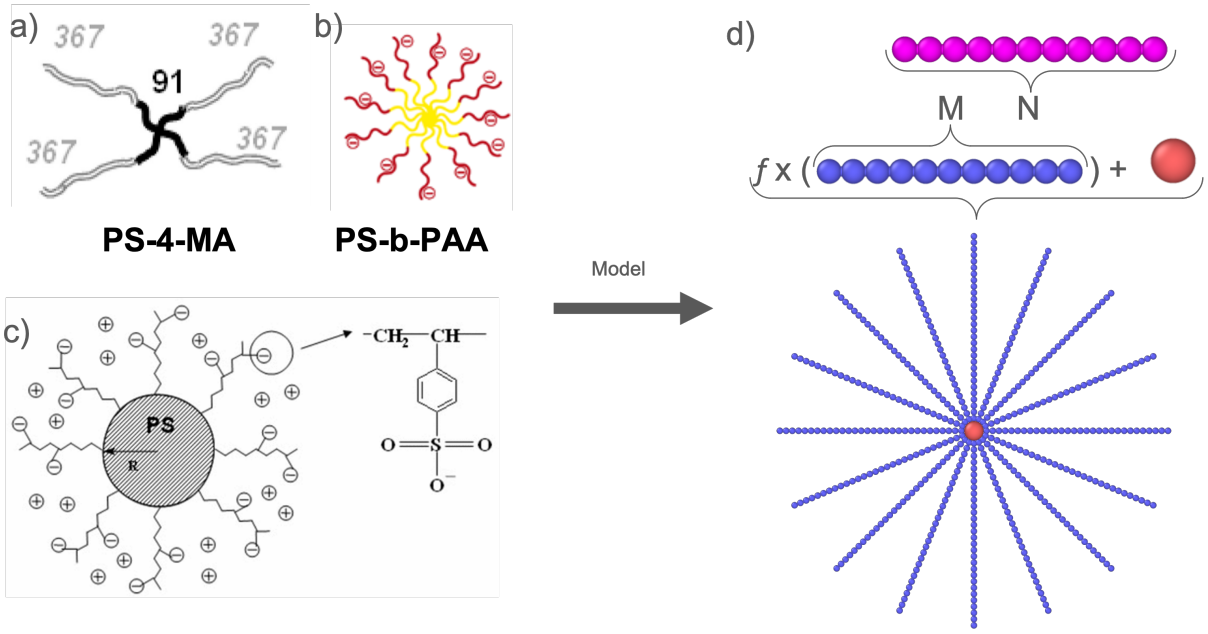

Figure 3.1: schematic representation of experimental systems represented by the model studied in this work. (a) Polystyrene core, methyl acrylate arms, star polymers by Raffa et al..[2] These assemble in micelles, increasing the core size and the number of arms. (b) diblock polystyrene-polyacrylamide assemblies by Maan et al..[21] (c) polystyrene colloidal particle with polystyrene sulfonate grafted on it by Mei et al..[34]. (d) representation of the architectural parameters f, M, N, that are respectively the functionality of a PE-GNP, length of PE-GNP arms and length of the LPE.

A harmonic potential is introduced to hold the particles and macromolecules together. The LJ potential is purely repulsive and arranges the volume exclusion effects in polymers. This potential will be both attractive and repulsive.[83]

$$U_h(r) = k(r - l_0)^2 \tag{3.4}$$

with $k = 2500\varepsilon_{LJ}/\sigma_{LJ}^2$, where the equilibrium bond length for monomer- monomer bonds is $l_0 = 1.0\sigma_{LJ}$ and for core monomer $l_0 = 1.5\sigma_{LJ}$. The equilibrium bond length and the shift in LJ potential determine the size of a bead. The larger equilibrium bond length and shifted LJ potential make the diameter of the core $2\sigma_{LJ}$.

The electrostatic interactions must be defined and incorporated as we are interested in charged particles. The charge of a single bead is set to the elementary charge, $q = 1e$, for all beads except for the neutral core. $q_{PE-GNP\,arm} = -1$; $q_{ion} = +1\ for\ \beta < 1$; $q_{ion} = -1\ for\ \beta > 1$; $q_{LPE} = +1$ The charge of a GNP is defined as follows: $Q_{GNP} = Mfq_{PE-GNP\,arm}$. For a single LPE, it is described as $Q_{LPE} = Nq_{LPE}$. The β parameter is defined as how much the charge of the GNP is compensated by the LPE or the degree of neutralization. To put it in a formula, which assumes a homogeneous distribution of LPE over the GNP, is as follows: $\beta = |Q_{\mathrm{LPE}} \cdot num_{\mathrm{LPE}}/Q_{\mathrm{PE-GNP}} \cdot num_{PE-GNP}|$. The Coulombic potential is defined below:[83]

$$U_{coul}(r) = \frac{C \cdot q_i \cdot q_j}{\varepsilon_{LJ} \cdot r} \quad \text{for } r < r_c \tag{3.5}$$

C is an energy conversion constant or energy scale. The charge screening properties of water are not considered in this potential. Other methods include debye screening for this cause. It is an added term in the shape of a decay exponential $\mathbf{e}^{-\kappa * \mathbf{r_{ij}}}$, with κ, the Debye length. This describes the screening effects of the medium. The Bjerrum length is related to the strength of an electrostatic interaction and the thermal energy. The dielectric constant is ε; this is changed to gauge the strength and robustness. The Bjerrum length is defined as $l_b = e^2/4\pi\varepsilon_0\varepsilon_r k_B T$ which was set to unity. ε_0 and ε_r are the vacuum's permittivity and the solvent's relative permittivity, and e is the elementary charge. These Coulomb interactions are calculated with the particle-particle-particle mesh (PPPM) approach; calculations are performed partly in real space (directly) and partly in reciprocal space (in kspace).[84] The Ewald value or accuracy set for this was 10^{-4}, the mesh size was 30 in all dimensions. The cutoff for that is $r_c = 10\sigma_{LJ}$

The size of the counterions is not feasible but necessary; realistic scales would break the simulation. Mass scales in a cubic fashion with bead radius while the forces on the counterions remain the same. One quickly enters a mass difference and, thus, an acceleration difference that nullifies the dynamics that are being studied. It would become a Born-Oppenheimer approximation that, instead of electrons, studies counterions.[85] The counterions are present for charge neutrality so that the PPM method can converge fully. Counterions are monovalent; LPE differs from multivalent counterions as LPE reaches much higher charge values while staying reasonable and has the added effect of paying a minor entropic penalty for aggregation. One could also add counterions for each component of the simulation cell. In this way, we get similar results, but the number of particles and simulation time is reduced significantly for simulations with increasing degrees of neutralization. Being aware of complex coaservation, studying a range of salt concentrations is possible and exciting. To avoid complicating the project in this way, only counterions for charge neutrality were studied

3.2 Simulation details

In all simulations, the number (64) and architecture 16 arms consisting of 30 Kuhn segments(f16-M30) of the PE-GNPS are kept constant. The contour length is defined as $L_c = M \cdot BondLength_{equillibrium}$. The red bead represents the core in the figure 3.1 and all other snapshots. Pink is LPE, blue is the arms of the GNP, and yellow counterions. All particles are randomly seeded into a box and compressed under NVT conditions according to the values in tables 3.1, 3.2. The concentration is based on the volume of the GNP beads and the box size: $c = V_{GNP}/Boxlength^3$. The boundaries of the box are periodic. $T = \varepsilon_{LJ}/k_B$ was set to unity. The time unit was defined as follows: $\tau_{LJ} = \sigma_{LJ}(m_{LJ}/\varepsilon_{LJ})^{\frac{1}{2}}$, where m is the mass, $m_{ion} = 1m_{LJ}$, and the same goes for the beads of LPE and PE-GNP arms. The mass of the core is $m_{core} = 8m_{LJ}$. The integration timestep is $\delta t = 0.005\tau_{LJ}$

$\sigma_{LJ} = 1$ nm approximately according to the Kuhn length.[18], [42] The values in this paper for persistence length seem rather different, 10 nanometers for low salt concentrations.[86] Kuhn length is two times the persistence length. However, this is an inherent quality of a polymer that is used for the model.

In this work, the degree of neutralization (charge ratio) β, N, the degree of polymerization of the linear polyelectrolytes, and c, the concentration, were varied. The concentration varies in the range c (vol%)= 10^{-2} - 5 and the corresponding box lengths. The degree of LPE polymerization is varied in the range of 2 - 50 beads. The degree of neutralization is in the range of 0.0 - 1.0 going from zero,

a bare star, to a stoichiometric $Q_{GNP} = Q_{LPE}$ elaborate depiction of the simulations, are given in the tables 3.1, 3.2. In most analyses, β is an input value, which assumes a homogeneous distribution of the LPE over the PE-GNP; however, this is not the case. When PE-GNP are investigated individually, they will correspond to the actual value.

This work is made under the Ergodic hypothesis.[87] If all relaxation times of the system are shorter than the simulation time and are in equilibrium, the microcanonical ensemble is equivalent to the time average. The sampling of generic thermodynamic $\langle A \rangle$ comes from the instantaneous value $A(t)$, in the following way[25]:

$$\langle A \rangle = \frac{1}{X} \sum_{j=1}^{X} A(t_0 + j\delta t) \tag{3.6}$$

This means that every frame can be regarded as a separate data point and weighed in on the standard error, making our sampling good enough to do fewer simulations.[88], [89] The equilibration time to test for substantial equilibration was the correlation of the end-to-end vector of the linear chain. In previous work, the relaxation of the PE-GNP was determined and deemed suitable.[50]

Table 3.1: simulation details Beta, constant architecture f16-M30 and LPE length N = 30

Concentrations (vol%)	**Degree of neutralization, β**
0.01	0.0, 0.1, 0.25, 0.4, 0.5, 0.6, 0.75, 0.9, 1.0, 1.5
0.1, 0.05, 0.25, 0.5	0.0, 0.1, 0.5, 0.75, 0.9, 1.0
1.0	0.0, 0.1, 0.25, 0.4, 0.5, 0.6, 0.75, 0.9, 1.0
3.0	0.0, 0.1, 0.5, 0.75, 0.9, 1.0, 1.5
5.0	0.1, 0.9, 1.0

Table 3.2: simulation details Degree of LPE polymerization, at β 0.0, 0.1, 0.5, 0.9, 1.0 (f16-M30)

Concentrations (vol%)	**degree of polymerization, *L***
0.01, 1.0	2, 5, 10, 20, 30, 40, 50
0.1	5, 10, 20, 30, 40, 50
0.05, 0.25, 0.5	30
3.0, 5.0	5, 10, 30, 50

3.3 Methodology

It takes multiple steps to arrive properly at the production run. This starts with randomly generating the PE-GNP in a box, followed by the LPE and counterions. The LPE is the number of PE-GNP arm beads multiplied by β, and the number of counterions is the number of PE-GNP arm beads minus the number of beads of LPE. Starting there are only LJ3.3 and harmonic3.4 potentials. A soft potential is introduced for non-bonded interactions to untangle overlapping molecules (NVT, $50\tau_{LJ}$). With this, the initial crashing of the simulation is prevented. As mentioned, the box length has been modified to match the correct size. This is done for $500\tau_{LJ}$ under NVE conditions and with the soft potential still.

Without the soft potential, the system is equilibrated for $50.000\tau_{LJ}$, NVT. This suffices for systems in solution and does not have a high polymer melt density. Followed by a further $500.000\tau_{LJ}$ under NVE. The charges are introduced over $500\tau_{LJ}$ and relaxed for another $500\tau_{LJ}$. Here, PE-GNP arms extend, and the LPEs condensate and coacervate with the PE-GNP, depending on concentration. This is enough time for the rearrangement of the PE-GNP and the association of the LPE. The aggregation of multiple PE-GNP is heavily time-dependent and does not happen over the whole following production run. That results in a production step of $50.000\tau_{LJ}$

To mitigate this effect, simulations run longer, and the time scale at which this happens is currently investigated. Multiple simulations would not improve the results, as the aggregation needs to happen (this is in the high degree of neutralization range).

The radius of gyration (R_g) indicates the size of the GNPs in the solution. This stems from the moment of inertia but is calculated as the square root of the average distance vector of all particles to a reference point. This reference point is the center of mass. To obtain this, we use the gyration tensor as Arkin and colleagues did; this results in Rg and the asphericity, a measure that indicates how spherical the particle or molecule is. [90]

Radial distribution functions (RDFs) provide information on the spatial distribution between particles by calculating how density varies as a function of distance from the reference. It also provides insight into the degree of ordering in the system with regular patterns indicating crystalline structure, for example. This was calculated using InterRDF, with the following equation[91], [92].

$$g_{ab}(r) = (N_a N_b)^{-1} \sum_{i=1}^{N_a} \sum_{j=1}^{N_b} \langle \delta(|\mathbf{r}_i - \mathbf{r}_j| - r) \rangle \tag{3.7}$$

Mean square displacement shows how the molecules' displacement evolves. This becomes useful when probing the caging dynamics of the GNP solution and obtaining diffusion coefficients. More information about the uniformity of the movement of the particles can be obtained. To calculate, Freud is used with the following equation[93]

$$MSD(m) = \frac{1}{N_{particles}} \sum_{i=1}^{N_{particles}} \frac{1}{N-m} \sum_{k=0}^{N-m-1} (\vec{r}_i(k+m) - \vec{r}_i(k))^2 \tag{3.8}$$

The end-to-end vector is the vector between the first and last particle of the LPE. This is calculated using numpy (array, positions, and inner). It gives an idea of the size of the polymer and how extended the polymer chains are. Especially when it is compared to the contour length (ℓ_c), this is the maximal length of a polymer chain with restricted angles between bonds or monomers. Our system does not pose such limitations on the polymer chains as this information is taken up in the Kuhn segment. The contour length is thus the number of monomers multiplied by the bond length.

Signac and Signac-flow Python packages were used for data management. [94], [95] Visualization of simulation trajectories and obtaining snapshots was achieved with Ovito.[96] Simulations were run with LAMMPS software.[53]

4 Results

4.1 Dilute Regime

To fully investigate the effects of the introduction of LPE on the phase behavior and shape of PE-GNP, the model has to be verified with current literature on a single PE-GNP. Therefore, the $\langle \mathbf{R_g} \rangle$ of the PE-GNP and where LPE and counterions are located will be discussed. The effects of the number of LPE, the degree of neutralization β, and their chain length, N, will be investigated. A single fixed particle in a box would have no interactions with other PE-GNP. It would approach an infinitely dilute solution, aside from the effect of the box walls or itself in periodic boundary conditions. Concentration is calculated as the PE-GNP's excluded volume divided by the volume of the simulation box. The values in the literature are ≈ 0.0004 vol% when the same principle is applied.[31], [32] The architectures, space position, and box lengths are summarized in table 4.1. They use different pair length values where one bead is more approximate to a small monomer. However, for $c = 10^{-3}$ vol%, unphysical behavior was seen in previous projects[50], and the PPPM was suggested as a possible problem for these box sizes and the number of particles. Therefore, the concentration that has been researched is two orders of magnitude higher, with a concentration of 0.01 vol%. This concentration remains in the dilute regime, and PE-GNP sizes correspond to previously found radius of gyration in the dilute limit, $\mathbf{R_g 0}$, values.

Architecture(f-16-M-30), the linear chain length at $N = 30$, core diameter $2\sigma_{LJ}$, and grafting density $1.27 arms/\sigma_{LJ}^2$ have been kept constant. Figure 4.1(a) shows how the PE-GNP collapses under the effect of neutralization by LPE. It is plotted with $\langle \mathbf{R_g} \rangle$ as a function of β, where the data points are averaged over all individual $\sqrt{R_g^2}$ calculations of PE-GNP and all timesteps. The error bars represent the standard error. The values for A somewhat quadratic decay can be observed for the brush thickness in a single particle simulation, with a minimum of $\beta = 1$.[31] This matches their mean-field theory model. This work focuses on the behavior of the whole particle; thus, the R_g that includes the particle's core is more sensible than the brush thickness. The values for the radius of gyration do not match, as is expected for a smaller core, less arms[33] and a larger core, more arms.[31]. What is comparable is how much the particle collapses. Both examples where R_g does not match reduce to $\sim 50\%$ of their original value. The same can be seen in this system's inset of figure 4.1(a). The

Table 4.1: Summary of architectures, box lengths, and simulation setups for other relevant works.

property	Mei et al.[32]	Ni et al.[31]	Larin et al.[33]	This work
Total numbers of particles	2401	2401	601	61504
Number of PE-GNPs	1	1	1	64
Arm length	30	30	30	30
Number of arms	40	40	10	16
Core radius	6	6	0.5	1
Pair length	$a = 0.2367$nm	$a = 0.25$nm	unspecified σ	$\sigma_{LJ} \approx 1$ nm
Box length	160	160	unspecified	546.85
Box boundaries	periodic	periodic	periodic	periodic
Particle position	fixed center	fixed center	fixed center	randomly seeded

trend of $\langle \mathbf{R_g} \rangle$ does not follow an equal trend as the brush thickness.[31] Towards $\beta = 1$ the collapse seems to be suppressed. Simulations of this work have further elucidated this. A quadratic decay occurs before $\beta = 0.9$, and afterward, its decay is dampened and nearing a plateau. The minimum is attained at $\beta = 1$. The origin of the collapse has been attributed to the loss of osmotic pressure as LPE replaces counterions. The nature has been identified as entropic as the same result is not seen for monovalent salt.[32], [34] They claim that condensated ions remain somewhat osmotically active, whereas multivalent ions are more strongly correlated, and their osmotic contribution is negligible. The more correlated, the smaller the osmotic contribution. This raises the hypothesis that longer LPE will have a larger effect on the $\langle \mathbf{R_g} \rangle$. This was found to be true for a single PE-GNP and multiple PE-GNPs. The effect of N does not continue infinitely and eventually plateaus. Figure 4.1 (b) shows that with increasing LPE length, the PE-GNP shrinks more. What was previously not shown is the dependence towards β for the plateau region. With increasing β, this is shifted to higher values of N. At low degrees of neutralization, there is barely any effect of LPE length, meaning it plateaus at $N = 2$. At a high degree of neutralization, the plateau has shifted to $N = 30$. This chain length was selected to achieve the maximal effect on the PE-GNPs while having the most number of chains and the most homogeneous behavior. Following from the distributions in the appendix A.1 where $N = 50$ more strongly favors narrow distributions towards no LPE in PE-GNPs. $N = 30$ performs better for this while maintaining a maximal impact for all studied β values.

In Mei et al. 2008, the Bjerrum length has been set to 3 a by a value of 7.1 Å. The Bjerrum length in the simulations of 1 σ_{LJ} equals the Kuhn length of a monomer, which should approach this value. In previous work, this has been approximated to $1\sigma_{LJ} = 1$ nm. This implies a Bjerrum length equal to 10 Å. This is overestimating the strength of the Coulombic interactions if one wants to simulate water at room temperature; calculating this for water would result in a temperature exceeding $100°C$. The shielding of water is not taken into account within the implicit solvent. One could add an exponential decay to the Coulombic potential to address the screening of water. Current efforts in systems where long-range electrostatics are relevant, such as bipolar nanopores, employ an all-atomistic explicit solvent representation of the system and a coarse-grained implicit solvent.[97] This is also done in protein simulations. [98]. The screening nature comes forth from the partial charges on oxygen and hydrogen, creating a dipole that screens charges.

The ratio of R_h and R_g was used to give more insight into the behavior and conformation of the PE-GNPs.[33] Typical values for a regular multiarm star are 0.93, and for a hard sphere, they are 1.29.[99] Upon increasing the degree of neutralization, the ratio R_h/R_g increased monotonously starting from 0.9, indicating a conformation more similar to a uniform hard sphere. Methods to calculate the hydrodynamic radius are with a single particle and not accessible for this work; this would have been valuable to estimate how compact the complexated PE-GNP and LPE are and help estimate the radius from R_g. [100]–[102]

Linear polyelectrolyte complexes of hyaluronic acid and chitosan hydrogels show the collapse when chains are not charged, a sharp increase when charged but not fully coacervated, towards a shrinkage once complexated that remains over a large pH range. [103] This was investigated with static light scattering, SLS.

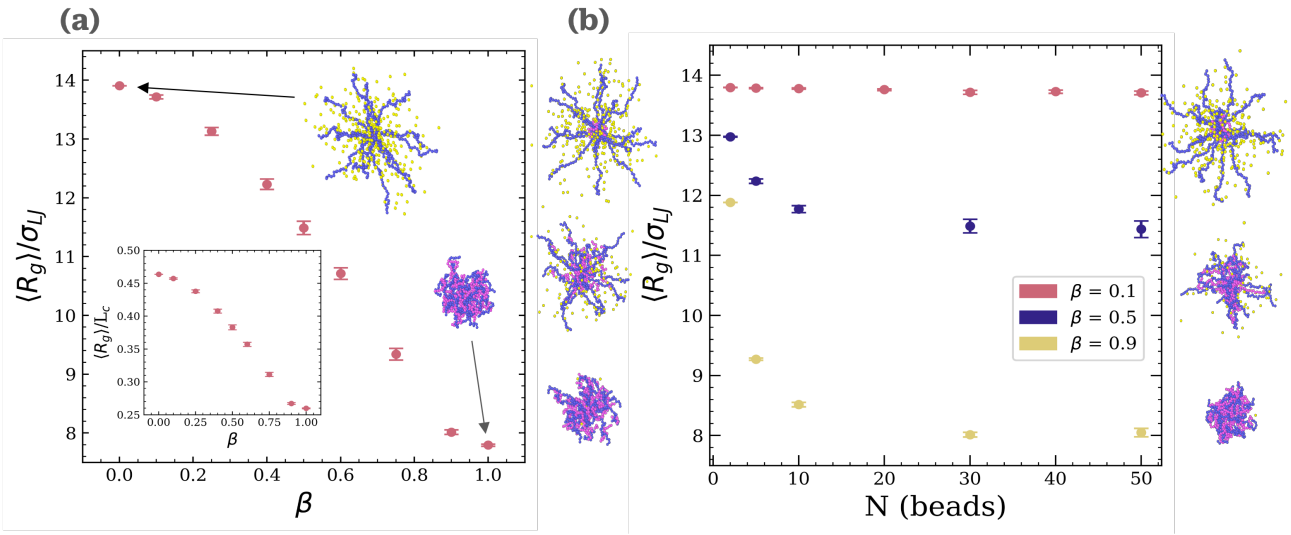

Figure 4.1: Description of the dilute regimes (0.01%) PE-GNP size ($\langle \mathbf{R_g} \rangle$). (a): The $\langle \mathbf{R_g} \rangle$ as a function of the degree of neutralization β, for constant LPE length $\mathbf{N = 30}$. This shows a stretched exponential, like $e^{-5/2}$, which comes close to its horizontal asymptote at $\beta = 0.9$. The snapshots belong to $\beta = 0.0$ and 1.0 (b): The $\langle \mathbf{R_g} \rangle$ as a function of the degree of polymerization, N, at varying degree of neutralization β. where the strength of the exponential decay depends on β. The insets on the left side of the figure are N = 5, and on the right side correspond to N = 50, from OVITO snapshots.

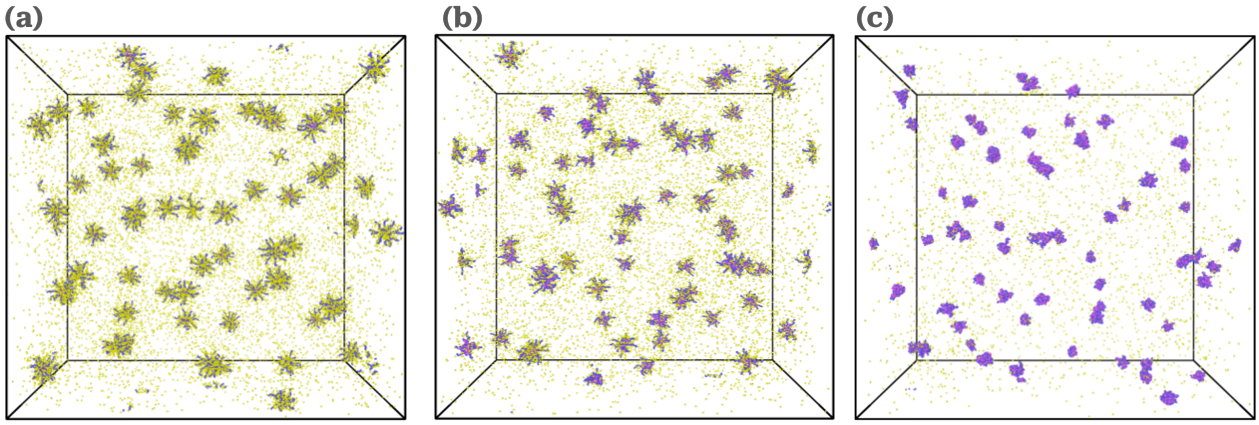

Figure 4.2: Simulation snapshots taken with OVITO, constant concentration $c = 0.01\%$ at different β: (a) $\beta = 0.1$, (b) $\beta = 0.5$, (c) $\beta = 0.9$. Red spheres (not visible) are the cores of the PE-GNPs, blue beads represent the Kuhn segments comprising the arms of the PE-GNPS, pink beads represent the LPE, and the yellow beads are counterions

Free linear chains cannot be seen in any of these snapshots. The literature confirms the denaturing behavior by comparing complexated linear chains to free linear chains. To show the denaturing effects, the $\langle R_g \rangle$ during charged is depicted in appendix A.2; this shows the denaturation of the LPE in dilute systems, where it is more stretched before complexation. In the overlap concentration, LPE is never free in solution, and upon charging, complexation is quicker than complete stretching of the LPE. The nature of these polymers can be further specified by characterizing the non-Gaussian parameter. The cores are strongly correlated, causing a high intensity; therefore, the peak at a higher length seemed

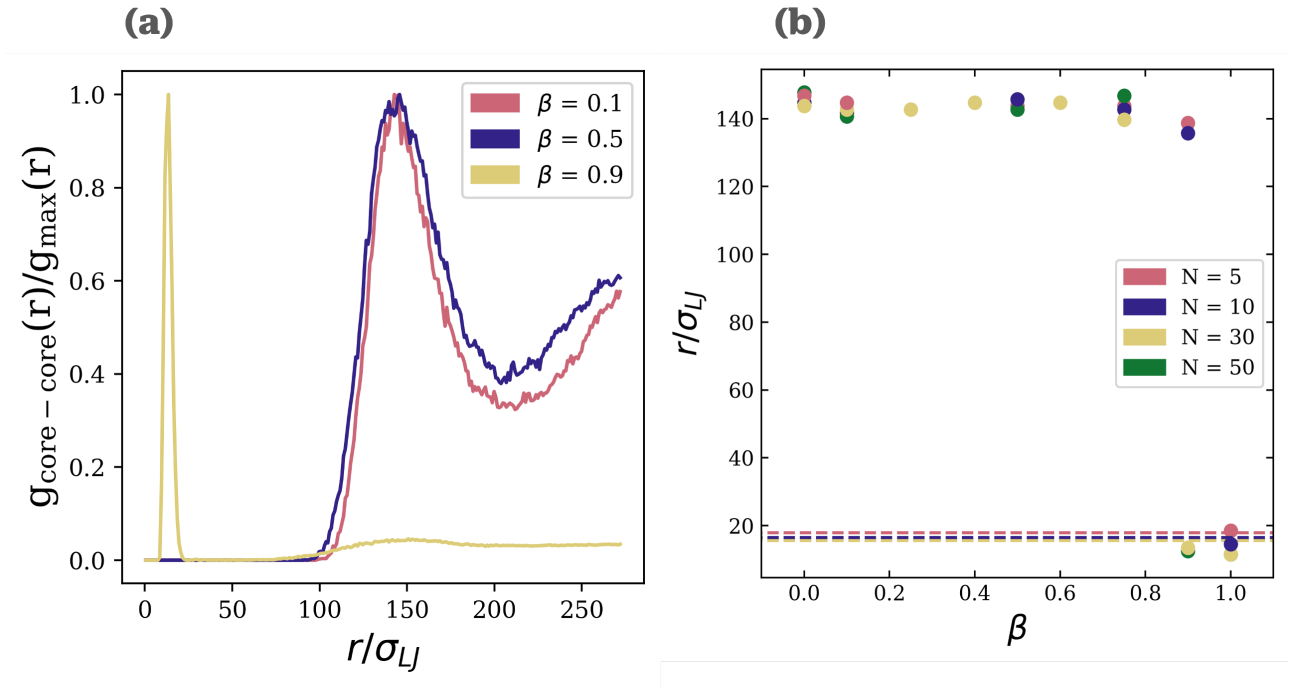

Figure 4.3: Radial distribution functions showing the association of multiple PE-GNP in the dilute regime. (a) The g(r) are plotted against r and are normalized for the maximal value. These show the correlation between the cores of the PE-GNP. The strong shift upon going to a high degree of neutralization is clear; the remaining peak, around 140, is less noticeable.

to have disappeared due to the normalization. The implications of this will be discussed further in the next chapter. Longer box length in this analysis could elucidate more of the structure of the second peak and indicate a glass or crystal structure. However, the MSD of the cores does not show a plateau indicating such structures. This is depicted in the appendix A.3

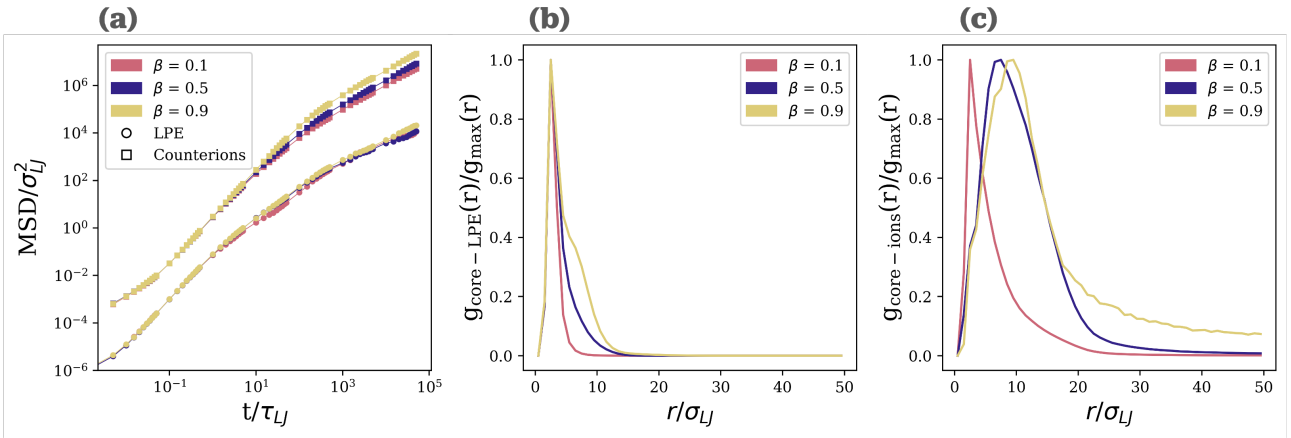

Figure 4.4: Mean square displacement and radial distribution functions in the dilute regime (c = 0.01 %) for N = 30. (a) mean square displacement showing that counterions are less associated with the slower PE-GNP at higher β values. (b) Shows how the linear chains are found within the Radius of the PE-GNP when β is increased. The peak broadens as more LPE are associated with the LPE and fill it radially. (c) Show the peak of the RDF shifting further away from the core. Also the the RDF does not become 0 for high neutralization, indicating for counterions, which are free to move, in solution.

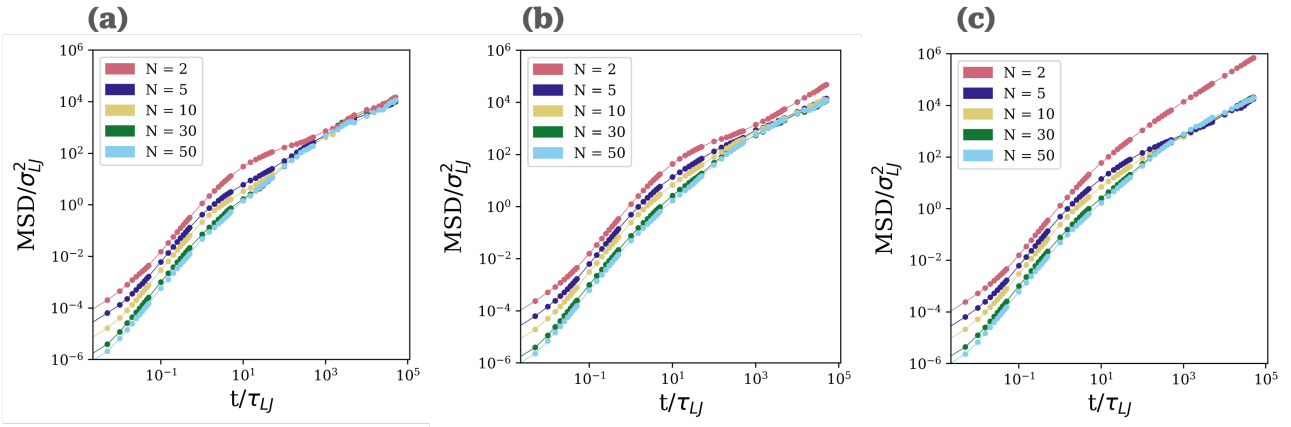

Figure 4.5: Mean square displacement at different degrees of neutralization for different chain lengths. (a) $\beta = 0.1$, (b) $\beta = 0.5$, (c) $\beta = 0.9$. Upon increasing β, the behavior of N = 2 diverges more. significantly diverging its behavior from the longer polyions. Increasing the degree of neutralization leads to earlier and more diffusive behavior, indicating a weaker correlation between LPE and PE-GNP

Looking at how the ions are distributed, it can be seen that they are shifted further away from the core and are also more common at farther distances. Further strengthening that the ions are becoming less osmotically active with increasing β. And complexation of LPE around the core pushing counterions out. The trend for linear chains is that they are situated as close to the core as possible, and when more LPE are in solution, this distribution widens but remains within the radius of the PE-GNP, meaning that they are not in solution.

The mean square displacement (MSD) shows no difference for the GNP in dilute systems in figure 4.2 when comparing different LPE lengths. For the ions, there is a larger difference. When more LPEs are added, the attractive electrostatic interaction between PE and counterion is weakened, and the ions are more free to move. The diffusion coefficient could be obtained as jusufi does in[37], [38], [104]. ions is $0.62\tau/a^2$, trivalent 0.11 and monomers 0.05 τ/a^2. Showing close approximation of the trivalent atoms towards the arms.

4.2 Overlap Regime

In the previously discussed dilute regime, PE-GNP behavior is mainly governed by the interaction between itself, counterions, and the LPEs (and solvent implicitly). Decreasing the simulation box size will force inter-PE-GNP interactions to occur. It will also increase the likelihood of LPEs interacting with multiple PE-GNP, potentially introducing bridging effects and coagulation.[31], [44] The effects of concentration are investigated with the previously explored parameters: degree of neutralization β and degree of LPE polymerization **N**. This introduces new fluctuation and correlation effects aside from electrostatics. The architecture will be kept constant, and aside from the investigation in LPE length, N will be kept constant, too.

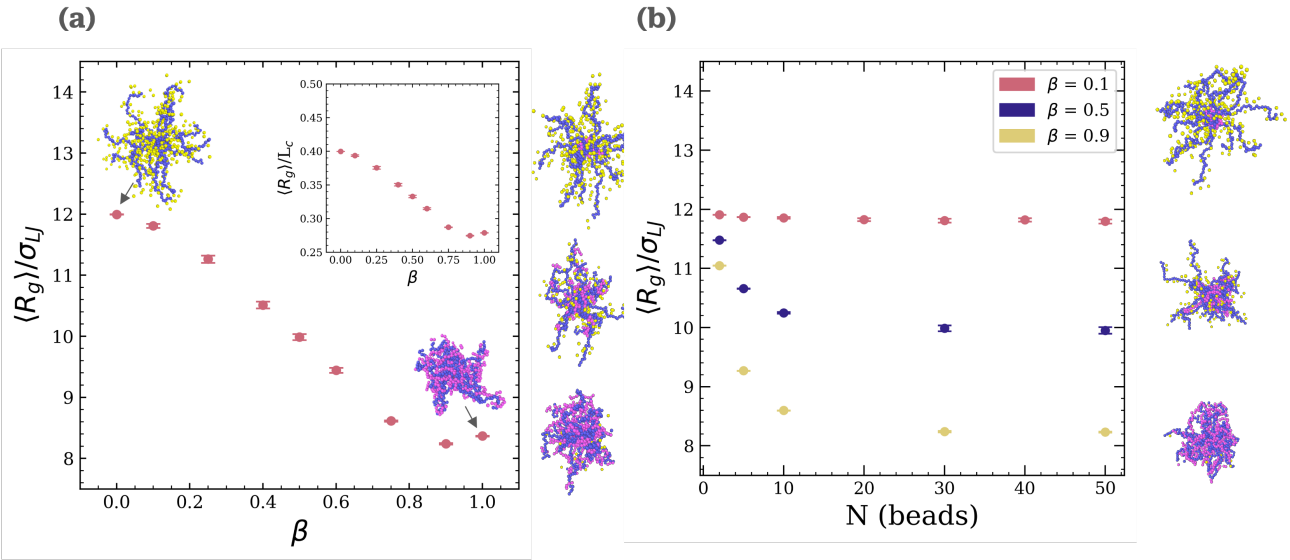

Figure 4.6: Description of the overlap regimes ($1vol\%$) PE-GNP size ($\langle \mathbf{R_g} \rangle$) and the distribution of LPE across the PE-GNPs. (a): The $\langle \mathbf{R_g} \rangle$ as a function of the degree of neutralization β, for constant LPE length $\mathbf{N = 30}$. This shows a stretched exponential, which comes close to its horizontal asymptote at $\beta = 0.9$. The snapshots belong to $\beta = 0.0$ and 1.0. (b): The $\langle \mathbf{R_g} \rangle$ as a function of the degree of polymerization, N, at varying the degree of neutralization β. where the strength of the exponential decay depends on β. The insets are on the left side of N = 5 and the right side of N = 50 from OVITO snapshots.

The effects and trends shown previously for a dilute system remain mainly present; adding more LPE leads to a smaller $\langle R_g \rangle$. The LPE-induced shrinking of the PE-GNPs is dampened as the whole system is already compressed. This holds at low β values where the $\langle \mathbf{R_g} \rangle$ decreases with about $2\sigma_{LJ}$ due to the concentration effects. The same shrinkage is not seen at high β values. The radius of gyration is slightly larger. More importantly from $\beta = 0.9$ to $\beta = 1.0$, the $\langle \mathbf{R_g} \rangle$ shows an increase in the $\langle \mathbf{R_g} \rangle$. This signals a more complex process involved in the shape control aside from the concentration-induced shrinkage [28] and LPE-induced collapse [31].

Until moderate degrees of neutralization in the dilute regime, LPEs remain condensated on the same PE-GNP. This is depicted in appendix A.4. This is also the case for higher degrees of neutralization initially. This does not continue, and the exchange of LPE happens throughout the rest of the simulation. When PE-GNPs are closer in the overlap regime, there is some exchange between the PE-GNPs. At $\beta = 0.9$, there is much more exchange of LPE. There is no initial absence of exchange as the aggregate has already been formed. This has also translated to the distribution of LPE. This gives the

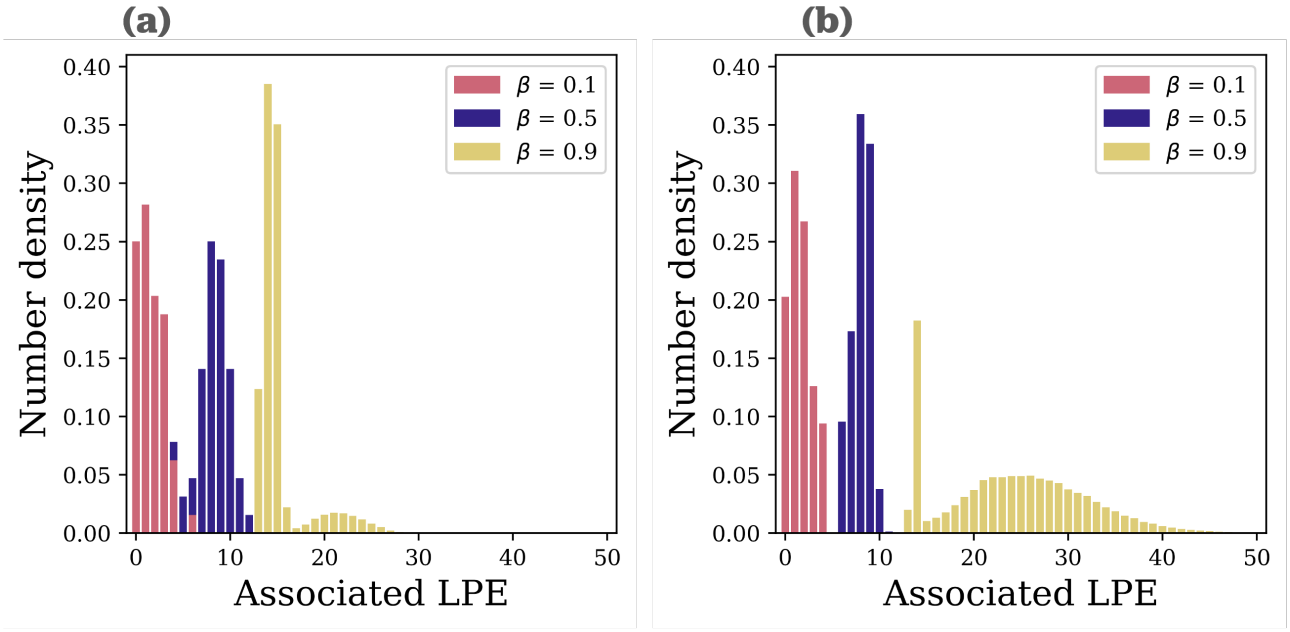

Figure 4.7: The distribution of LPE of PE-GNP over the whole simulation. An LPE is counted as associated if one of the beads is inside a sphere with an approximated radius from the R_g and the degree of neutralization. (a) dilute regime, 0.01 vol%, (b) overlap regime, 1.0 vol%

sharp distribution for $\beta = 0.1$ and 0.5, independent of the concentration. Two different distributions at a high degree of neutralization indicate two different states of PE-GNP LPE complexation. These are sharp distributions similar to those of lower neutralization systems and a much smoother and broader distribution. The former indicates the LPE being stuck in the PE-GNP. The latter suggests that LPEs are somewhat free to redistribute themselves among the PE-GNPs. This relates to the dimerized and fully coagulated states for respective dilute and overlap concentrations with a high degree of neutralization. A single PE-GNP is more common than dimerized PE-GNPs in the dilute regime. For the overlap concentration, the agglomerate is predominant.

At low β, the distribution includes PE-GNPs that do not have LPE condensation within them. This affects the behavior and should be noted; however, the scale of effects seen at higher β values does not seem significant. There seems to be overlapping PE-GNP; this can be a 3d effect where they are behind one another in space. However, with this and the distribution of LPE in 4.2. The hypothesis that complete neutralization aggregation occurs and LPEs are shared between multiple PE-GNPs seems likely. In the dilute regime, these PE-GNP do not interact; however, still, some interaction happens, and in 10 τ, these dimers form; going more dilute would probably circumvent this, as PE-GNP do not coalesce further.

The distribution further insinuates that there is interpenetration as the two confirmation sets with and without interpenetration have shifted more towards the interpenetration one. Meaning more linear chains inside. There are still PE-GNPs that do not have this interaction as strongly.

Typical concentration-driven shrinking in the overlap regime has a slope of -1/3; for a semidilute electrostatic regime, this is -1/4 without condensation of counterions or LPE. This typical decrease is when polyelectrolyte stars get so compressed that the particles can not compress further and must

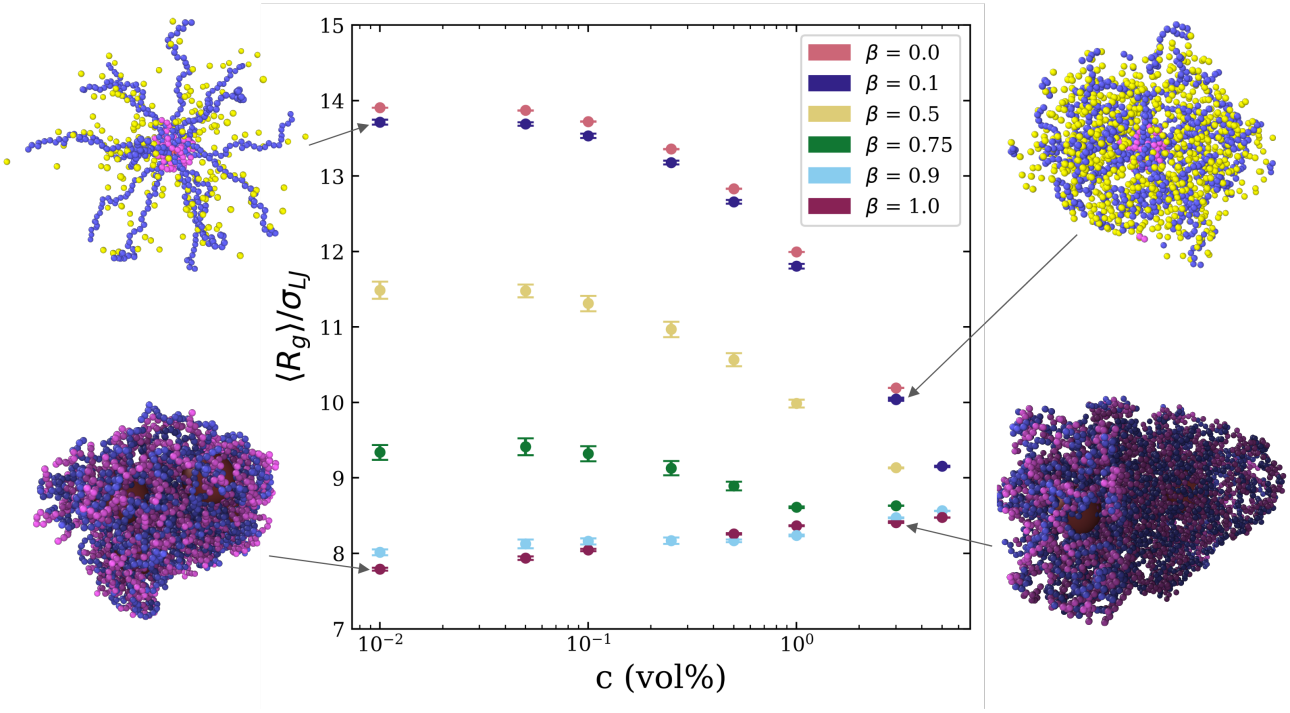

Figure 4.8: (a): Average values for the $\mathbf{R_g}$ as a function of concentration. (b): average asphericity of PE-GNP as a function concentration. Introducing LPE shifts the size behavior from interdigitation avoidance to interpenetration-driven swelling of the PE-GNP. The shape, however, is not affected by either concentration or β. The inset shows a PE-GNP and its environment. The left side is in the dilute regime, and the right side is in the overlap regime. The top left shows a single PE-GNP with condensated LPE and both condensated and uncondensated counterions. When more LPEs are added, dimerization can occur in the dilute regime. This is depicted in the bottom left, where the core size is exaggerated to show the presence of two PE-GNP. On the bottom right, more than one PE-GNP is depicted. The added shading is important as this is part of a larger agglomerate. The light side is on the outside, and the darker areas are on the inside. The top right shows a single PE-GNP, but in the overlap concentration, this is completely surrounded by the arms of other PE-GNP and counterions.

interpenetrate to accompany one another. When concentration is increased enough, it will become constant in figure 4.8. Two trends can be seen. Below $\beta = 0.75$, a constant dilute regime shifts into the overlap regime where the particle collapses.[50] Above $\beta = 0.75$ a gradual increase in $\langle \mathbf{R_g} \rangle$. Further cementing that the behavior shifts upon agglomeration. At high β, chains interdigitate and extend more due to the favorable interaction between LPEs and PE-GNPs. At $\beta = 0.75$, there seems to be a turnover in the behavior, where until c = 1 vol% shows overlap behavior, the $\langle \mathbf{R_g} \rangle$ decreases with increasing concentration. Above this concentration, it shows an increase instead of a further collapse. This could indicate that the turnover point of most PE-GNPs are complexated. It can also be that the minimum size of the PE-GNP has been reached. Increasing the concentration further will show if this is due to the concentration effects plateauing out and reaching quasineutral semidilute regimes or if the agglomeration is dominant. The overlap concentration, c*, is defined as the intersection of the linear fit for the dilute regime and overlap regime, corresponding to the PE-GNP arms touching. The LPE-dampened concentration effects in the overlap regime shift this to lower concentrations. This does not fit in as the particles are smaller and expected to have an overlap concentration at a higher concentration than PE-GNPs with altered architecture.

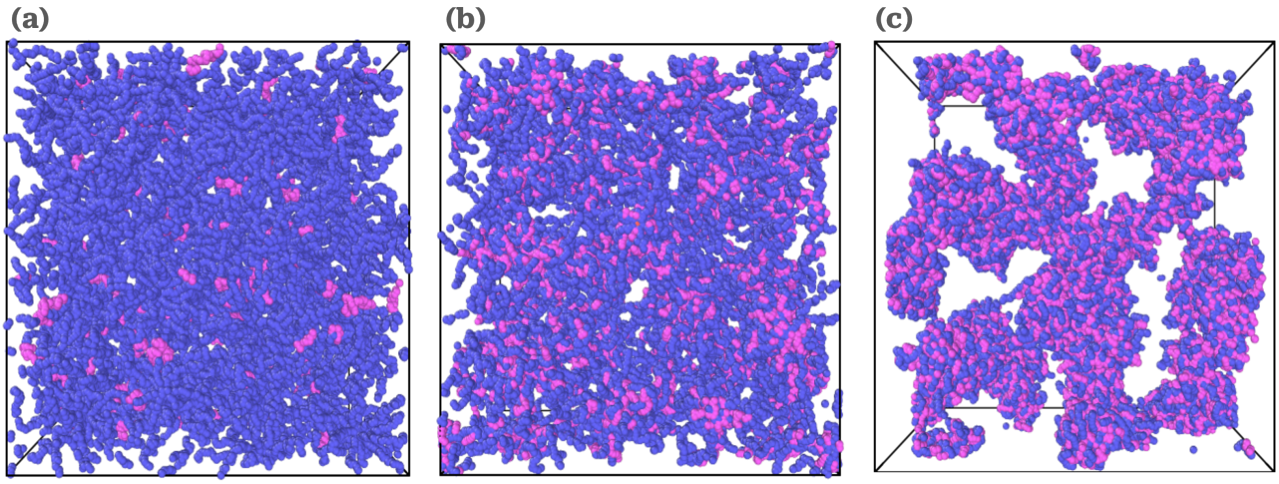

Figure 4.9: Simulation snapshots taken with OVITO, constant concentration $c = 1\%$ at different β: (a) $\beta = 0.1$, (b) $\beta = 0.5$, (c) $\beta = 0.9$. Red spheres (not visible) are the cores of the PE-GNPs, blue beads represent the Kuhn segments comprising the arms of the PE-GNPS, pink beads represent the LPE, and counterions are omitted for clarity.

What is important to note is that the PE-GNPs do not become more spherical or aspherical with increasing concentration. A fully extended star has been reported to be more spherical, with a lower value for asphericity.[105] The asphericity is plotted against concentration for various degrees of neutralization in Appendix A.5. Concentration and aggregation do not make a meaningful difference in the asphericity, and the number of associated LPE does not either.

The snapshots show that the particles have agglomerated. At a low degree of neutralization, the simulation box is occupied by PE-GNP. When more LPEs are present, the system shows empty space. Empty space is because of the implicit solvent and would constitute the supernatant phase. The inter-core distance is a good indication of the aggregation of the PE-GNP. This is not visible from the snapshot. Therefore, the first RDF peaks between the PE-GNP cores are introduced to show the proximity of the PE-GNP. This shows a sharp decrease in the length between the cores when the number of LPE is increased. This is also dependent on the LPE length. N = 10, 30, and 50 transitions before $\beta = 0.9$. N = 5 transitions after $\beta = 0.9$. This has changed from the dilute system and N = 10 transitions at lower β. The correlation between cores shifts to shorter lengths for values lower than twice the $\langle R_g \rangle$ and much more than twice the characteristic radius, R. Indicating the interpenetration of PE-GNPs. This is further confirmed by linear chains interacting with multiple PE-GNPs. Around $\beta = 1.0$, this phenomenon induces this behavior for all LPE lengths.

The MSD is similar to the one previously displayed for the dilute system in figure 4.4, where linearity is achieved. In figure 4.11, the MSD of LPEs does not become linear. At $\beta = 0.1$, a plateau at the end of the simulation is seen. This is an indication of a glass or crystal structure. Longer simulations are necessary to explore this effect further. Counterions are uncondensed and remain mobile. The RDF shows the same trends as the dilute system; LPEs are closest to the core, and counterions are pushed out further. The neighboring PE-GNP and its associated LPE and counterions are representing the second peak shown for both LPE and counterions.

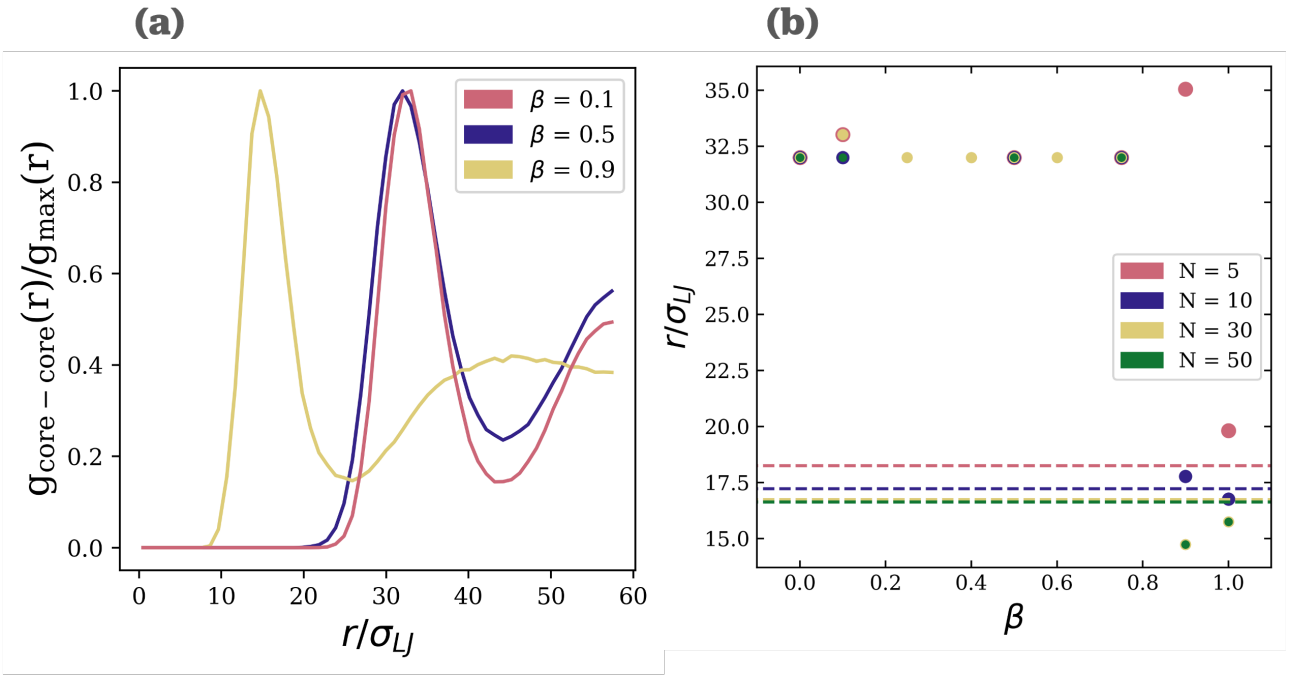

Figure 4.10: The figures describe the shrinkage of the inter-core distances at c = 1.0 %. (a) shows the RDF between cores. (b) shows the location on the x-axis for the first peak in Figure (a) for multiple LPE lengths.

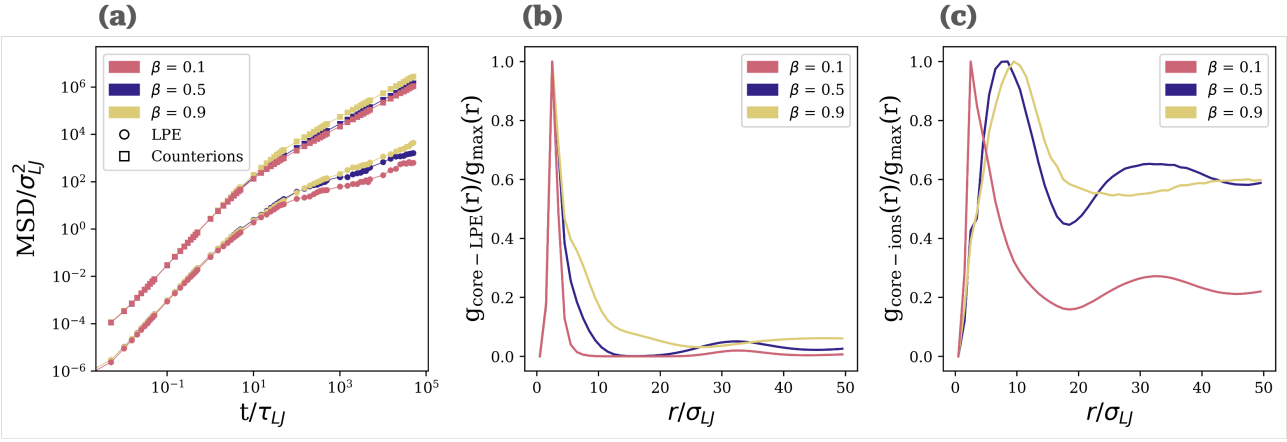

Figure 4.11: Mean square displacement and radial distribution functions in the overlap regime (c = 1 vol%) for N = 30. (a) mean square displacement showing that counterions are free at higher β values. (b) also shows this, as well as the counterions being further away from the core. (c) shows how the linear chains are inside the PE-GNP and fill it up more and more when β is increased.

4.3 general discussion

When increasing the LPE in solution, this $\mathbf{R_{g0}}$ is strongly influenced, similarly to changing whole architectures. Before aggregation is induced by LPE, this is an effective way to tune the viscosity and shift the non-linear rheological response. For these β values, soft colloidal rheology is a good descriptor. The particles do not get meaningfully deformed by the addition of LPE, which would suggest the behavior shifting to more polymer-like. When aggregation happens at high degrees of neutralization, the system behaves as a complex coacervate. This changes the rheological response to that of a crosslinked network with temporary crosslinks originating from the charged interactions. LPE association is expected to be tunable with salt concentration in both cases. Increasing the salt concentration leading to the screening of the charges and minimizing the entropic and enthalpic gain of the solvent, similar to complex coacervation of LPEs.

Two states are distributed at high β and dilute concentration, the sharp distribution indicating non-aggregated PE-GNP and the broader one PE-GNP that are aggregated. There is an exchange of LPE between these PE-GNP, also when they are not fully aggregated and only dimerized. Dimerization allows for the interchange of LPE between PE-GNPS. It also takes on the characteristic semidilute behavior. The distance between the cores is smaller than the PE-GNP's radius or the brush's length. Indicating interpenetration of the arms. However, the behavior will remain colloidal, as discussed in the previous paragraph.

This is a quantitative model; one needs a more sophisticated method and proper parameterization for more qualitative predictions. Without going all atomistic, one can introduce ion-dipole $\sim 1/r^4$ interaction potentials and accompanying induced or permanent dipoles. Coase-grained models will not suffice to capture effects originating from chirality, hydrogen bonding, and solvation. The current model provides the basis for adding more and more system-specific interactions.

Simulating the appropriate time to achieve reliable results from the equilibrium state is needed. There is an inversion of the effective potential between PE-GNPs for high beta. Depending on the concentration, this leads to an aggregation or phase separation with a different timescale. High-concentration systems assemble instantaneously; lower-concentration systems do not. This is known. However, dimerization occurs only in the first 5% of the simulation. Thus, the system will still be treated as if it were in equilibrium. The system tends to crystallize in other group work; these timescales are not explored. Longer simulations did not show more aggregation, and further investigation will focus on compressing and decompressing the system. This will show if the aggregate forms and if it will hold. The MSD of the dimer system shows no signal of a long-range vitrified state, preventing further agglomeration. With regards to uncovering the size and shape of the PE-GNP, it matters for particles to be in solution or as coacervate and need to be studied; there is already a model showing the coacervate, and this model at higher concentration.

Further characterization of the system, which is currently not present, is the average end-to-end vector of the PE-GNP arms, which could give an accurate value for the thickness of the brush. R_g is still a more experimentally accessible alternative, but the average end-to-end vector could be used to verify the estimation of the PE-GNP radius based on R_g. Although it may break down in the overlap regime depending on the arm contraction. The non-Gaussian parameter could be introduced to specify the uniformity of behavior of PE-GNP, LPE, and counterions. Contact analysis of the LPE with the PE-GNP elucidates how these interact. Surface area analysis could further cement the complex

coacervation when the surface area is minimalized. The complex coacervation can be further explored and compared to phase diagrams. It is expected to have a narrow area that shows phase separation. Coupling this with the viscosity of soft particles and complex coacervates has the potential for 3d printing of polyelectrolytes.

LPE longer than $N = 30$ attaches near the center of the core, as shown in the RDF. In this work, we do not push the limit or compare it to common complex coacervation where chains have a similar amount of charges. However, results similar to those of hybrid coacervation might arise when there is more charge than one PE-GNP.[44] Here, the LPE is bridging the space between colloids. Simulating longer linear chains than the charge of a single PE-GNP could be interesting and hard to predict with the current results.

The future of this research will focus on combining changes in architecture and the addition of LPE. Some unexplored gaps remain. Pushing the limit of LPE length would allow LPE to interact with multiple PE-GNP at a lower degree of neutralization. The previously mentioned further exploration of the aggregation, mainly with compression, the dielectric constant, and the effect of water screening. Pushing the limit of multivalent ions further, although unrealistic, could provide more insight into the workings of the system and the impact of entropy.

5 Conclusion

This work has presented the control of the size and shape of polyelectrolyte grafted nanoparticles, PE-GNPs, with the addition of linear polyelectrolytes, LPEs, to the solution. The coarse-grained molecular dynamics model of the PE-GNP has built upon single PE-GNP simulations and architecture studies of multiple PE-GNPs. The role of the degree of neutralization was studied concerning the structural configuration, showing the collapse of PE-GNPs as previously shown in the literature. Up to a degree of neutralization of 0.75, a collapse of the PE-GNP is seen, while overlap behavior, typical of star polymers, remains. At higher degrees of neutralization, previously hypothesized aggregation occurs. In the dilute regime, this leads to dimerization. Above the overlap concentration, the whole system aggregates. This aggregation decreases the inter-core distance to below that of the radius of the PE-GNP, achieving semidilute behavior at concentrations below the transition to the semidilute regime. This was shown with the RDF, and the interdigitation of PE-GNPs was confirmed. Interdigitation of PE-GNP, without LPE, is only seen in the semidilute regime. A hint of glass formation is seen at $c = 1.0$ vol% for low degrees of neutralization. This is inhibited when the degree of neutralization is higher. Combining the effects of LPE and concentration shows that both effects are simultaneously present. Analysis of the LPE length effect shows the importance of the degree of neutralization, β shifts the plateau in R_g induced at longer chain length to higher values. This is compressed into the notice of the dynamic behavior of the solution, which is well described by soft colloidal solutions, with size-related jamming being important. When the PE-GNP aggregate, the dynamical behavior is better described as a complex coacervate governed by temporary electrostatic crosslinks.

Relevant areas and current gaps in this work are in a broader range of LPE lengths ($N \leq \pm 480$) that show the effect of LPE that can fully neutralize a PE-GNP or induce PE-GNP aggregation at a lower degree of neutralization. A systematic investigation beyond complete neutralization ($\beta \geq 1.0$) will show the disaggregation of the PE-GNP. This potentially leads to a narrow phase diagram that fully describes these systems. To study this, it is essential to have a better understanding of the long-scale dynamics. This is to elucidate the complexation time scale and link the PE-GNP's size and shape to the polyelectrolyte solutions' dynamic state. The estimation of the Bjerrum length being larger than room temperature water and the absence of screening of water could present future challenges. Future work will further explore this line of research for different PE-GNP architectures.

Acknowledgments

The micromechanics group has opened its arms to me, and I am most grateful to all. Dr. Andrea Giuntoli created this welcoming environment, which is truly wonderful. I want to thank him for his insights, support, and advice in challenging times. The freedom and tools to learn, challenge, and further develop myself at my own pace have been enjoyable. Although he still owes me a chess game, the work is as finished as it will be.

Utku Gürel, my daily supervisor, explained so much code and solved many problems and bugs, for which I am very grateful. The discussion and guidance have been very valuable for this research project.

The group, especially Savio and Johan, gave me great feedback. These two have shown me all the cool things they know in Python, terminal, and Overleaf.

References

[1] C. Chen and T. Weil, "Cyclic polymers: synthesis, characteristics, and emerging applications," *Nanoscale Horizons*, vol. 7, no. 10, pp. 1121–1135, Sep. 2022.

[2] P. Raffa, P. Brandenburg, D. A. Wever, A. A. Broekhuis, and F. Picchioni, "Polystyrene-poly(sodium methacrylate) amphiphilic block copolymers by ATRP: Effect of structure, pH, and ionic strength on rheology of aqueous solutions," *Macromolecules*, vol. 46, no. 17, pp. 7106–7111, Sep. 2013.

[3] P. Raffa, D. A. Z. Wever, F. Picchioni, and A. A. Broekhuis, "Polymeric Surfactants: Synthesis, Properties, and Links to Applications," *Chemical reviews*, vol. 115, no. 16, pp. 8504–8563, Aug. 2015.

[4] R. S. Yu and S. Singh, "Microplastic Pollution: Threats and Impacts on Global Marine Ecosystems," *Sustainability 2023, Vol. 15, Page 13252*, vol. 15, no. 17, p. 13 252, Sep. 2023.

[5] C. J. Hu, M. A. Garcia, A. Nihart, *et al.*, "Microplastic presence in dog and human testis and its potential association with sperm count and weights of testis and epididymis," *Toxicological Sciences*, May 2024.

[6] L. Lebreton, B. Slat, F. Ferrari, *et al.*, "Evidence that the Great Pacific Garbage Patch is rapidly accumulating plastic," *Scientific Reports*, vol. 8, no. 1, p. 4666, Dec. 2018.

[7] K. Moraczewski, "Modification and Processing of Biodegradable Polymers," *Modification and Processing of Biodegradable Polymers*, p. 324, May 2023.

[8] F. Schmid, "Understanding and Modeling Polymers: The Challenge of Multiple Scales," *ACS Polymers Au*, vol. 3, no. 1, pp. 28–58, Feb. 2023.

[9] B. Zhang, R. Wepf, K. Fischer, *et al.*, "The Largest Synthetic Structure with Molecular Precision: Towards a Molecular Object," *Angewandte Chemie International Edition*, vol. 50, no. 3, pp. 737–740, Jan. 2011.

[10] S. P. Danielsen, H. K. Beech, S. Wang, *et al.*, "Molecular Characterization of Polymer Networks," *Chemical Reviews*, vol. 121, no. 8, pp. 5042–5092, Apr. 2021.

[11] B. Crist and J. M. Schultz, "Polymer spherulites: A critical review," *Progress in Polymer Science*, vol. 56, pp. 1–63, May 2016.

[12] Y. Li, B. C. Abberton, M. Kröger, and W. K. Liu, "Challenges in Multiscale Modeling of Polymer Dynamics," *Polymers 2013, Vol. 5, Pages 751-832*, vol. 5, no. 2, pp. 751–832, Jun. 2013.

[13] M. Ballauff, "Spherical polyelectrolyte brushes," *Progress in Polymer Science*, vol. 32, no. 10, pp. 1135–1151, Oct. 2007.

[14] A. Jusufi, C. N. Likos, and M. Ballauff, "Counterion distributions and effective interactions of spherical polyelectrolyte brushes," *Colloid and Polymer Science*, vol. 282, no. 8, pp. 910–917, Jun. 2004.

[15] B. M. Erwin, M. Cloitre, M. Gauthier, and D. Vlassopoulos, "Dynamics and rheology of colloidal star polymers," *Soft Matter*, vol. 6, no. 12, pp. 2825–2833, Jun. 2010.

[16] D. Vlassopoulos and M. Cloitre, "Tunable rheology of dense soft deformable colloids," *Current Opinion in Colloid & Interface Science*, vol. 19, no. 6, pp. 561–574, Dec. 2014.

[17] G. Petekidis, D. Vlassopoulos, and P. N. Pusey, "Yielding and flow of sheared colloidal glasses," *Journal of Physics: Condensed Matter*, vol. 16, no. 38, S3955, Sep. 2004.

[18] R. A. M. Yunus, U. Gürel, A. Guzik, *et al.*, "Glass Transition and Yielding of Ultrasoft Charged Spherical Micelles," *Unpublished*,

[19] M. Seth, A. Ramachandran, B. P. Murch, and L. G. Leal, "Origins of microstructural transformations in charged vesicle suspensions: The crowding hypothesis," *Langmuir*, vol. 30, no. 34, pp. 10 176–10 187, Sep. 2014.

[20] L. Michorius and F. Picchioni, "Differently structured polystyrene-b-poly(methacrylic acid) polymeric micelles and their possible use as a pH sensitive drug delivery system Motivation for the research," Ph.D. dissertation, RuG, 2022.

[21] A. M. Maan, C. N. Graafsma, A. H. Hofman, T. Pelras, W. M. de Vos, and M. Kamperman, "Scalable Fabrication of Reversible Antifouling Block Copolymer Coatings via Adsorption Strategies," *ACS Applied Materials and Interfaces*, vol. 15, no. 15, pp. 19 682–19 694, Apr. 2023.

[22] W. Xu, P. A. Ledin, V. V. Shevchenko, and V. V. Tsukruk, "Architecture, Assembly, and Emerging Applications of Branched Functional Polyelectrolytes and Poly(ionic liquid)s," *ACS Applied Materials and Interfaces*, vol. 7, no. 23, pp. 12 570–12 596, Jun. 2015.

[23] J. P. Hallett and T. Welton, "Room-temperature ionic liquids: Solvents for synthesis and catalysis. 2," *Chemical Reviews*, vol. 111, no. 5, pp. 3508–3576, May 2011.

[24] C. Zhao, J. Zhang, J. Lv, *et al.*, "Development of Novel Star-Like Branched-Chain Acrylamide (AM)-Sodium Styrene Sulfonate (SSS) Copolymers for Heavy Oil Emulsion Viscosity Reduction and Its Potential Application in Enhanced Oil Recovery," *ACS Omega*, vol. 9, no. 1, pp. 422–436, Jan. 2024.

[25] M. Rubinstein and R. Colby, *Polymer Physics Introduction*. Oxford University Press, 2003.

[26] C. E. Sing and S. L. Perry, "Recent progress in the science of complex coacervation," *Soft Matter*, vol. 16, no. 12, pp. 2885–2914, Mar. 2020.

[27] L. A. Smook and S. de Beer, "Electrical Chain Rearrangement: What Happens When Polymers in Brushes Have a Charge Gradient?" *Langmuir*, Feb. 2024.

[28] N. P. Shusharina and M. Rubinstein, "Concentration regimes in solutions of polyelectrolyte stars," *Macromolecules*, vol. 41, no. 1, pp. 203–217, Jan. 2008.

[29] C. N. Likos, N. Hoffmann, A. Jusufi, and H. Löwen, "Interactions and phase behaviour of polyelectrolyte star solutions," *Journal of Physics: Condensed Matter*, vol. 15, no. 1, S233, Dec. 2002.

[30] C. Mayer and C. N. Likos, "A coarse-grained description of star-linear polymer mixtures," *Macromolecules*, vol. 40, no. 4, pp. 1196–1206, Feb. 2007.

[31] R. Ni, D. Cao, W. Wang, and A. Jusufi, "Conformation of a spherical polyelectrolyte brush in the presence of oppositely charged linear polyelectrolytes," *Macromolecules*, vol. 41, no. 14, pp. 5477–5484, Jul. 2008.

[32] Y. Mei, M. Hoffmann, M. Ballauff, and A. Jusufi, "Spherical polyelectrolyte brushes in the presence of multivalent counterions: The effect of fluctuations and correlations as determined by molecular dynamics simulations," *Physical Review E - Statistical, Nonlinear, and Soft Matter Physics*, vol. 77, no. 3, p. 031 805, Mar. 2008.

[33] S. V. Larin, A. A. Darinskii, E. B. Zhulina, and O. V. Borisov, "Interpolyelectrolyte complexes between starlike and linear macromolecules: A structural model for nonviral gene vectors," *Langmuir*, vol. 25, no. 4, pp. 1915–1918, Feb. 2009.

[34] Y. Mei, K. Lauterbach, M. Hoffmann, O. V. Borisov, M. Ballauff, and A. Jusufi, "Collapse of Spherical Polyelectrolyte Brushes in the Presence of Multivalent Counterions," *Physical review letters*, vol. 97, no. 158301, pp. 1–4, 2006.

[35] R. P. Pothukuchi, V. K. Prajapat, and M. Radhakrishna, "Charge-Driven Self-Assembly of Polyelectrolyte-Grafted Nanoparticles in Solutions," *Langmuir*, vol. 37, no. 41, pp. 12 007–12 015, Oct. 2021.

[36] J. J. Zhang and B. Li, "Self-Assembly of Star-Polyelectrolytes in Various Solution Conditions," *Macromolecules*, vol. 57, no. 1, pp. 396–408, Jan. 2024.

[37] H. M. Harreis, C. N. Likos, and M. Ballauff, "Can dendrimers be viewed as compact colloids? A simulation study of the fluctuations in a dendrimer of fourth generation," *The Journal of Chemical Physics*, vol. 118, no. 4, pp. 1979–1988, Jan. 2003.

[38] I. O. Götze and C. N. Likos, "Conformations of Flexible Dendrimers: A Simulation Study," *Macromolecules*, vol. 36, no. 21, pp. 8189–8197, Oct. 2003.

[39] W. D. Tian and Y. Q. Ma, "Molecular dynamics simulations of a charged dendrimer in multivalent salt solution," *Journal of Physical Chemistry B*, vol. 113, no. 40, pp. 13 161–13 170, Oct. 2009.

[40] Y. H. Tang, Z. Li, X. Li, M. Deng, and G. E. Karniadakis, "Non-Equilibrium Dynamics of Vesicles and Micelles by Self-Assembly of Block Copolymers with Double Thermoresponsivity," *Macromolecules*, vol. 49, no. 7, pp. 2895–2903, Apr. 2016.

[41] Q. Cao, C. Zuo, L. Li, and M. Gao, "Interactions of polyelectrolyte brushes with oppositely charged surfactants," *Colloid and Polymer Science*, vol. 289, no. 10, pp. 1089–1102, Apr. 2011.

[42] C. Gioldasis, L. N. Gergidis, and C. Vlahos, "Micellization through complexation of oppositely charged diblock copolymers: Effects of composition, polymer architecture, salt of different valency, and thermoresponsive block," *Journal of Polymer Science*, vol. 59, no. 2, pp. 191–204, Jan. 2021.

[43] A. Kalogirou, L. N. Gergidis, K. Miliou, and C. Vlahos, "Complexation of Polyelectrolyte Micelles with Oppositely Charged Linear Chains," *Journal of Physical Chemistry B*, vol. 121, no. 8, pp. 1982–1991, Mar. 2017.

[44] A. M. Rumyantsev, O. V. Borisov, and J. J. De Pablo, "Structure and Dynamics of Hybrid Colloid-Polyelectrolyte Coacervates," *Macromolecules*, vol. 56, no. 4, pp. 1713–1730, Feb. 2023.

[45] B. Yu, H. Liang, P. F. Nealey, M. V. Tirrell, A. M. Rumyantsev, and J. J. de Pablo, "Structure and Dynamics of Hybrid Colloid-Polyelectrolyte Coacervates: Insights from Molecular Simulations," *Macromolecules*, vol. 56, no. 18, pp. 7256–7270, Sep. 2023.

[46] A. Chremos and J. F. Douglas, "Communication: When does a branched polymer become a particle?" *Journal of Chemical Physics*, vol. 143, no. 11, Sep. 2015.

[47] Q. H. Hao, G. Xia, H. G. Tan, E. Q. Chen, and S. Yang, "Surface morphologies of spherical polyelectrolyte brushes induced by trivalent salt ions," *Physical Chemistry Chemical Physics*, vol. 20, no. 41, pp. 26 542–26 551, Oct. 2018.

[48] R. Faller, "Coarse-Grain Modeling of Polymers," *Reviews in Computational Chemistry*, vol. 23, pp. 233–262, 2007.

[49] S. Y. Joshi and S. A. Deshmukh, "A review of advancements in coarse-grained molecular dynamics simulations," *Molecular Simulation*, vol. 47, no. 10-11, pp. 786–803, Jul. 2021.

[50] I. A. Gjerapić, "Characterizing Structural Conformation of Diblock Star-polyelectrolyte Micelles and its Concentration Dependence Utilizing Molecular Dynamics Simulations," Ph.D. dissertation, RuG, 2023, pp. 1–32.

[51] S. Kmiecik, D. Gront, M. Kolinski, L. Wieteska, A. E. Dawid, and A. Kolinski, "Coarse-Grained Protein Models and Their Applications," *Chemical Reviews*, vol. 116, no. 14, pp. 7898–7936, Jul. 2016.

[52] R. Shi, H. J. Qian, and Z. Y. Lu, "Coarse-grained molecular dynamics simulation of polymers: Structures and dynamics," *Wiley Interdisciplinary Reviews: Computational Molecular Science*, vol. 13, no. 6, e1683, Nov. 2023.

[53] A. P. Thompson, H. M. Aktulga, R. Berger, *et al.*, "LAMMPS - a flexible simulation tool for particle-based materials modeling at the atomic, meso, and continuum scales," *Computer Physics Communications*, vol. 271, p. 108 171, Feb. 2022.

[54] R. Zwanzig, "Theoretical basis for the Rouse-Zimm model in polymer solution dynamics," *The Journal of Chemical Physics*, vol. 60, no. 7, pp. 2717–2720, Apr. 1974.

[55] J. J. Hermans and R. Stein, "Polymer solution properties. Part II. Hydrodynamics and light scattering," *Journal of Polymer Science: Polymer Letters Edition*, vol. 17, no. 2, pp. 105–105, Feb. 1979.

[56] P. J. Flory and T. G. Fox, "Treatment of Intrinsic Viscosities," *Journal of the American Chemical Society*, vol. 73, no. 5, pp. 1904–1908, 1951.

[57] P. J. Flory, *Principles of Polymer Chemistry*. Cornell University Press, 1953.

[58] M. Daoud, J. P. Cotton, B. Farnoux, *et al.*, "Solutions pf Flexible Polymers. Neutron Experiments and Interpretation," *Macromolecules*, vol. 6, no. 22, p. 2251, 1973.

[59] M. Daoud and G. Jannink, "Temperature-concentration diagram of polymer solutions.," *Journal de Physique II*, vol. 37, no. 7-8, pp. 973–979, 1976.

[60] M. Daoud and J. P. Cotton, "Star shaped polymers : a model for the conformation and its concentration dependence," *Journal de Physique*, vol. 43, no. 3, pp. 531–538, 1982.

[61] D. Vlassopoulos and M. Cloitre, "Suspensions of Soft Colloidal Particles," *Theory and Applications of Colloidal Suspension Rheology*, pp. 227–290, Apr. 2021.

[62] A. M. Rumyantsev, E. B. Zhulina, and O. V. Borisov, "Surface-Immobilized Interpolyelectrolyte Complexes Formed by Polyelectrolyte Brushes," *ACS Macro Letters*, vol. 12, no. 12, pp. 1727–1732, Dec. 2023.

[63] G. S. Manning, "Limiting Laws and Counterion Condensation in Polyelectrolyte Solutions I. Colligative Properties," *The Journal of Chemical Physics*, vol. 51, no. 3, pp. 924–933, Aug. 1969.

[64] A. Jusufi, C. N. Likos, and H. Löwen, "Counterion-induced entropic interactions in solutions of strongly stretched, osmotic polyelectrolyte stars," *The Journal of Chemical Physics*, vol. 116, no. 24, pp. 11 011–11 027, Jun. 2002.

[65] J. Rühe, M. Ballauff, M. Biesalski, *et al.*, *Polyelectrolyte Brushes*. Springer, Berlin, Heidelberg, 2004, pp. 79–150.

[66] N. Dingenonts, M. Patel, S. Rosenfeldt, D. Pontoni, T. Narayanan, and M. Ballauff, "Counterion distribution around a spherical polyelectrolyte brush probed by anomalous small-angle X-ray scattering," *Macromolecules*, vol. 37, no. 21, pp. 8152–8159, Oct. 2004.

[67] B. Das, X. Guo, and M. Ballauff, "The osmotic coefficient of spherical polyelectrolyte brushes in aqueous salt-free solution," *Progress in Colloid and Polymer Science*, vol. 121, pp. 34–38, 2002.

[68] S. Chen and Z. G. Wang, "Driving force and pathway in polyelectrolyte complex coacervation," *Proceedings of the National Academy of Sciences of the United States of America*, vol. 119, no. 36, Sep. 2022.

[69] S. Varner, C. Balzer, and Z. G. Wang, "Entropic Origin of Ionic Interactions in Polar Solvents," *Journal of Physical Chemistry B*, vol. 127, p. 4337, 2023.

[70] S. Chen and Z. G. Wang, "Charge Asymmetry Suppresses Coarsening Dynamics in Polyelectrolyte Complex Coacervation," *Physical Review Letters*, vol. 131, no. 21, p. 218 201, Nov. 2023.

[71] A. M. Rumyantsev, E. B. Zhulina, and O. V. Borisov, "Complex Coacervate of Weakly Charged Polyelectrolytes: Diagram of States," *Macromolecules*, vol. 51, no. 10, pp. 3788–3801, May 2018.

[72] C. Y. Lemetter, F. M. Meeuse, and N. J. Zuidam, "Control of the morphology and the size of complex coacervate microcapsules during scale-up," *AIChE Journal*, vol. 55, no. 6, pp. 1487–1496, Jun. 2009.

[73] B. Yu, A. M. Rumyantsev, N. E. Jackson, *et al.*, "Complex coacervation of statistical polyelectrolytes: role of monomer sequences and formation of inhomogeneous coacervates," *Molecular Systems Design & Engineering*, vol. 6, no. 10, pp. 790–804, Oct. 2021.

[74] B. Peng and M. Muthukumar, "Modeling competitive substitution in a polyelectrolyte complex," *Journal of Chemical Physics*, vol. 143, no. 24, p. 243 133, Dec. 2015.

[75] E. Spruijt, M. A. Cohen Stuart, and J. Van Der Gucht, "Linear viscoelasticity of polyelectrolyte complex coacervates," *Macromolecules*, vol. 46, no. 4, pp. 1633–1641, Feb. 2013.

[76] H. Bohidar, P. L. Dubin, P. R. Majhi, C. Tribet, and W. Jaeger, "Effects of protein - Polyelectrolyte affinity and polyelectrolyte molecular weight on dynamic properties of bovine serum albumin - Poly(diallyldimethylammonium chloride) coacervates," *Biomacromolecules*, vol. 6, no. 3, pp. 1573–1585, May 2005.

[77] O. A. Balashova, A. S. Pavlov, and P. G. Khalatur, "Polyampholyte solutions in the presence of salts: A stochastic dynamics study," *Polymer Science - Series A*, vol. 49, no. 3, pp. 314–319, Mar. 2007.

[78] S. Wang, Z. Li, and W. Pan, "Implicit-solvent coarse-grained modeling for polymer solutions via Mori-Zwanzig formalism," *Soft Matter*, vol. 15, no. 38, pp. 7567–7582, Oct. 2019.

[79] X. Qiang, X. Wang, Y. Ji, S. Li, and L. He, "Liquid-crystal self-assembly of lipid membranes on solutions: A dissipative particle dynamic simulation study," *Polymer*, vol. 115, pp. 1–11, Apr. 2017.

[80] G. S. Grest, "Structure of Many-Arm Star Polymers in Solvents of Varying Quality: A Molecular Dynamics Study," *Macromolecules*, vol. 27, no. 13, pp. 3493–3500, Jun. 1994.

[81] G. S. Grest, K. Kremer, and T. A. Witten, "Structure of Many-Arm Star Polymers: A Molecular Dynamics Simulation," *Macromolecules*, vol. 20, no. 6, pp. 1376–1383, Nov. 1987.

[82] M. J. Stevens and K. Kremer, "The nature of flexible linear polyelectrolytes in salt free solution: A molecular dynamics study," *The Journal of Chemical Physics*, vol. 103, no. 4, pp. 1669–1690, Jul. 1995.

[83] A. Chremos and J. F. Douglas, "Solution properties of star polyelectrolytes having a moderate number of arms," *The Journal of chemical physics*, vol. 147, no. 4, p. 044 906, Jul. 2017.

[84] R. Hockney and J. Eastwood, *Computer simulation using particles*, 1st. CRC, 1988.

[85] P. Atkins and R. Friedman, "Molecular Quantum Mechanics," in *Molecular Quantum Mechanics*, 5th, New York: Oxford University Press, 2011, ch. 8, pp. 258–260.

[86] M. N. Spiteri, F. Boué, A. Lapp, and J. P. Cotton, "Polyelectrolyte persistence length in semidilute solution as a function of the ionic strength," *Physica B: Condensed Matter*, vol. 234-236, pp. 303–305, Jun. 1997.

[87] R. D. Skeel, "WHAT MAKES MOLECULAR DYNAMICS WORK?" *SIAM journal on scientific computing : a publication of the Society for Industrial and Applied Mathematics*, vol. 31, no. 2, p. 1363, Jan. 2009.

[88] E. Braun, J. Gilmer, H. B. Mayes, *et al.*, "Best Practices for Foundations in Molecular Simulations," *Living journal of computational molecular science*, vol. 1, no. 1, 2019.

[89] A. Grossfield, P. N. Patrone, D. R. Roe, A. J. Schultz, D. Siderius, and D. M. Zuckerman, "Best Practices for Quantification of Uncertainty and Sampling Quality in Molecular Simulations," *Living journal of computational molecular science*, vol. 1, no. 1, 2018.

[90] H. Arkin and W. Janke, "Gyration tensor based analysis of the shapes of polymer chains in an attractive spherical cage," *Journal of Chemical Physics*, vol. 138, no. 5, p. 54 904, Feb. 2013.

[91] R. J. Gowers, M. Linke, J. Barnoud, *et al.*, "MDAnalysis: A Python Package for the Rapid Analysis of Molecular Dynamics Simulations," *Proceedings of the 15th Python in Science Conference*, pp. 98–105, 2016.

[92] N. Michaud-Agrawal, E. J. Denning, T. B. Woolf, and O. Beckstein, "MDAnalysis: A toolkit for the analysis of molecular dynamics simulations," *Journal of Computational Chemistry*, vol. 32, no. 10, pp. 2319–2327, Jul. 2011.

[93] B. D. Dice, V. Ramasubramani, E. S. Harper, M. P. Spellings, J. A. Anderson, and S. C. Glotzer, "Analyzing Particle Systems for Machine Learning and Data Visualization with freud," *Proceedings of the 18th Python in Science Conference*, pp. 27–33, 2019.

[94] V. Ramasubramani, C. S. Adorf, P. M. Dodd, B. D. Dice, and S. C. Glotzer, "signac: A Python framework for data and workflow management," *Proceedings of the 17th Python in Science Conference*, pp. 152–159, 2018.

[95] C. S. Adorf, P. M. Dodd, V. Ramasubramani, and S. C. Glotzer, "Simple Data and Workflow Management with the signac Framework," *Computational Materials Science*, vol. 146, pp. 220–229, Nov. 2016.

[96] A. Stukowski, "Visualization and analysis of atomistic simulation data with OVITO–the Open Visualization Tool," *Modelling and Simulation in Materials Science and Engineering*, vol. 18, no. 1, p. 015 012, Dec. 2009.

[97] A. Córdoba, J. M. de Oca, S. B. Darling, and J. J. de Pablo, "Influence of the Dielectric Constant on the Ionic Current Rectification of Bipolar Nanopores," *ACS Nano*, vol. 18, no. 19, pp. 12 569–12 579, 2024.

[98] V. Adupa, E. Ustyantseva, H. H. Kampinga, and P. R. Onck, "Tertiary structure and conformational dynamics of the anti-amyloidogenic chaperone DNAJB6b at atomistic resolution," *Nature Communications 2024 15:1*, vol. 15, no. 1, pp. 1–12, Apr. 2024.

[99] W. Burchard, "Solution Properties of Branched Macromolecules," *Advances in Polymer Science*, vol. 143, pp. 113–194, 1999.

[100] M. Nygaard, B. B. Kragelund, E. Papaleo, and K. Lindorff-Larsen, "An Efficient Method for Estimating the Hydrodynamic Radius of Disordered Protein Conformations," *Biophysical journal*, vol. 113, no. 3, pp. 550–557, Aug. 2017.

[101] A. I. Grosberg and A. R. Khokhlov, *Statistical physics of macromolecules*. AIP Press, 1994, p. 350.

[102] L. B. Weiss, V. Dahirel, V. Marry, and M. Jardat, "Computation of the Hydrodynamic Radius of Charged Nanoparticles from Nonequilibrium Molecular Dynamics," *Journal of Physical Chemistry B*, vol. 122, no. 22, pp. 5940–5950, Jun. 2018.

[103] G. Lalevée, L. David, A. Montembault, *et al.*, "Highly stretchable hydrogels from complex coacervation of natural polyelectrolytes," *Soft Matter*, vol. 13, no. 37, pp. 6594–6605, Sep. 2017.

[104] A. Jusufi, "Fluctuation effects and monomer-counterion correlations in starlike polyelectrolyte systems," *Journal of Chemical Physics*, vol. 124, no. 4, p. 44 908, Jan. 2006.

[105] U. Gürel and A. Giuntoli, "Shear Thinning from Bond Orientation in Model Unentangled Bottlebrush Polymer Melts," *Macromolecules*, vol. 56, no. 15, pp. 5708–5717, Aug. 2023.

Appendices

A Additional analysis

The radius of the star is estimated from the R_g by accounting for the packing of the star, in comparison to a hard sphere and a fully extended star. These have a respective conversion factor to the radius of 1.29 and 1.75. These are estimated to scale linearly with the density of the particle, where the hard sphere has a density of 1.

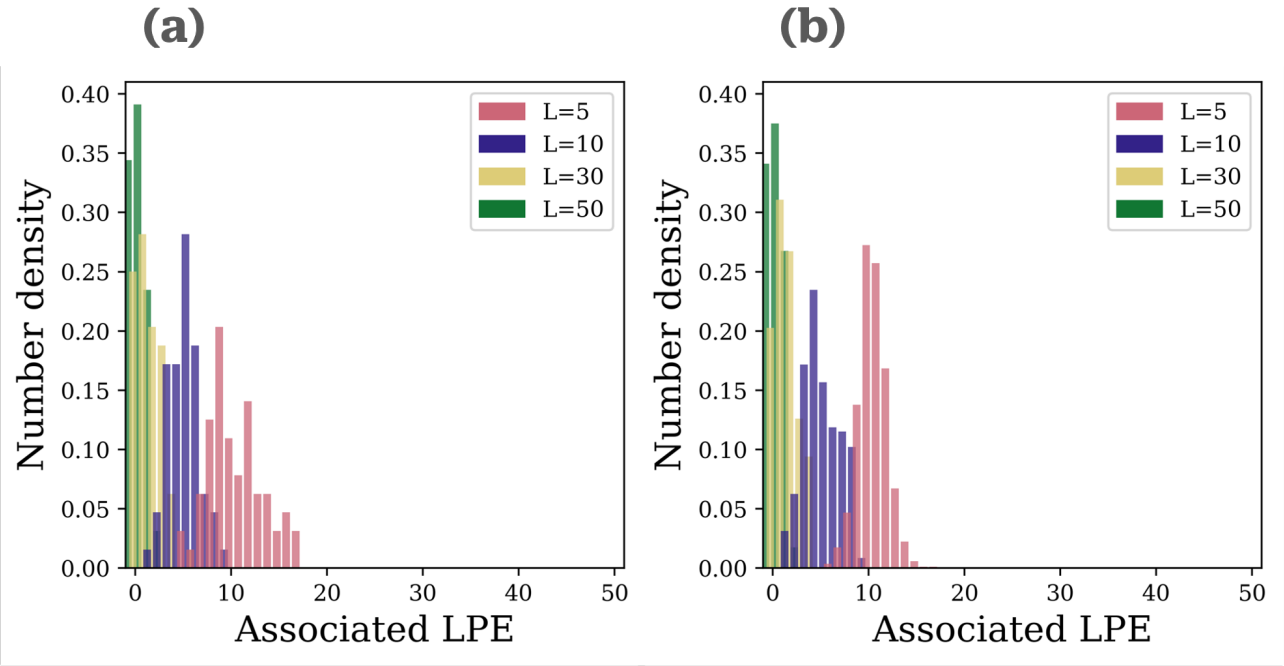

Figure A.1: Distribution of LPE over the PE-GNP, every chain length is shifted to show every bar without overlap. (a) dilute regime 0.01 vol%, (b) overlap regime 1.0 vol%

There are more linear chains at $\beta = 0.9$, which indicates the changes in figure A.4. A normalized version does not make sense; this is about general activity. For $\beta = 0.9$ it is 921, $\beta = 0.5$ 512, $\beta = 0.1$ 102.

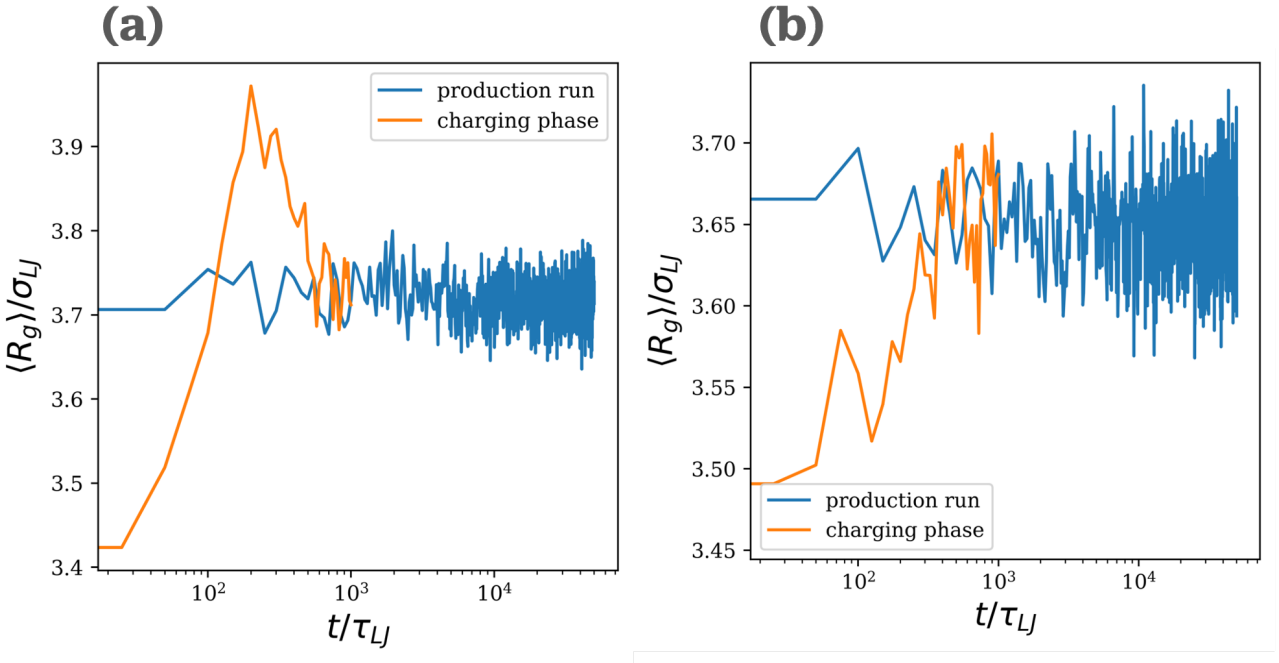

Figure A.2: plot of $\langle R_g \rangle$ of LPE versus time. The charging phase is the 500τ where all charges are ramped from 0e to 1e and subsequently relaxed for 500τ. The production run is when the system is charged, and regular data is acquired. (a) dilute regime 0.01 vol%, showing an increase in $\langle R_g \rangle$, stretched conformation, before complexation occurs and the LPE denatures (b) overlap regime 1.0 vol% LPE complexes are formed before going to a stretched state.

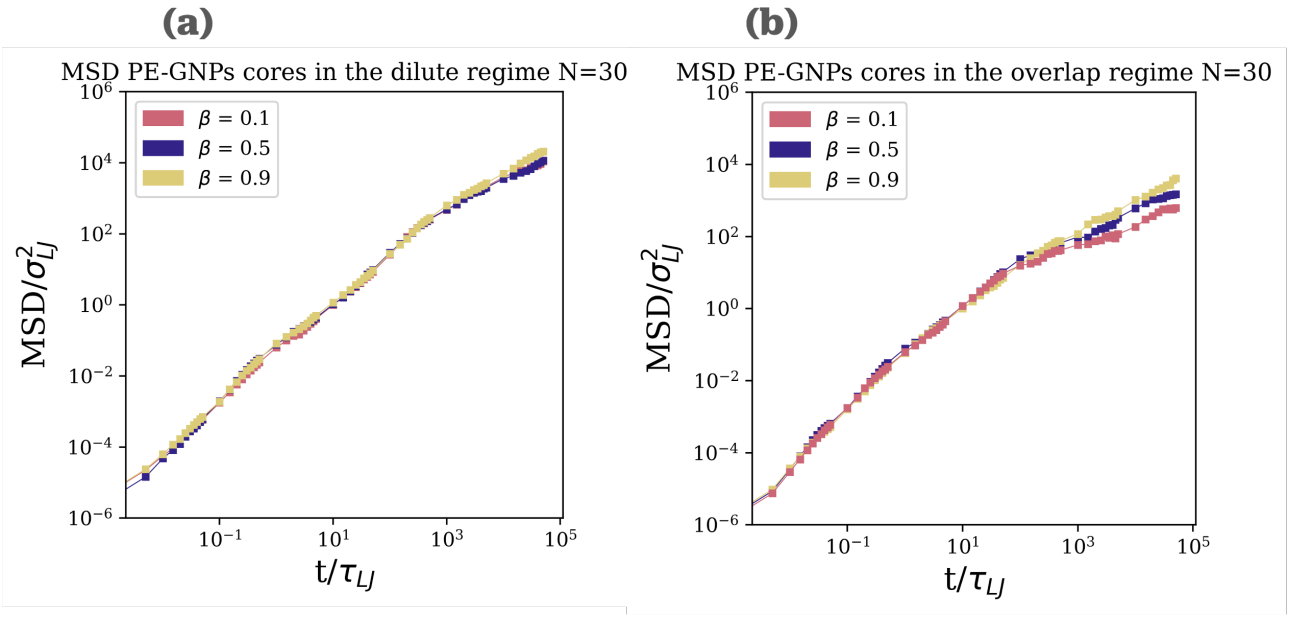

Figure A.3: MSD of the core of the PE-GNP, approaching linearity towards the end of the simulation and diffusivity. (a) dilute regime 0.01 vol%, (b) overlap regime 1.0 vol% there is a hint of a plateau in the MSD for low degree of neutralization, that would indicate glass formation

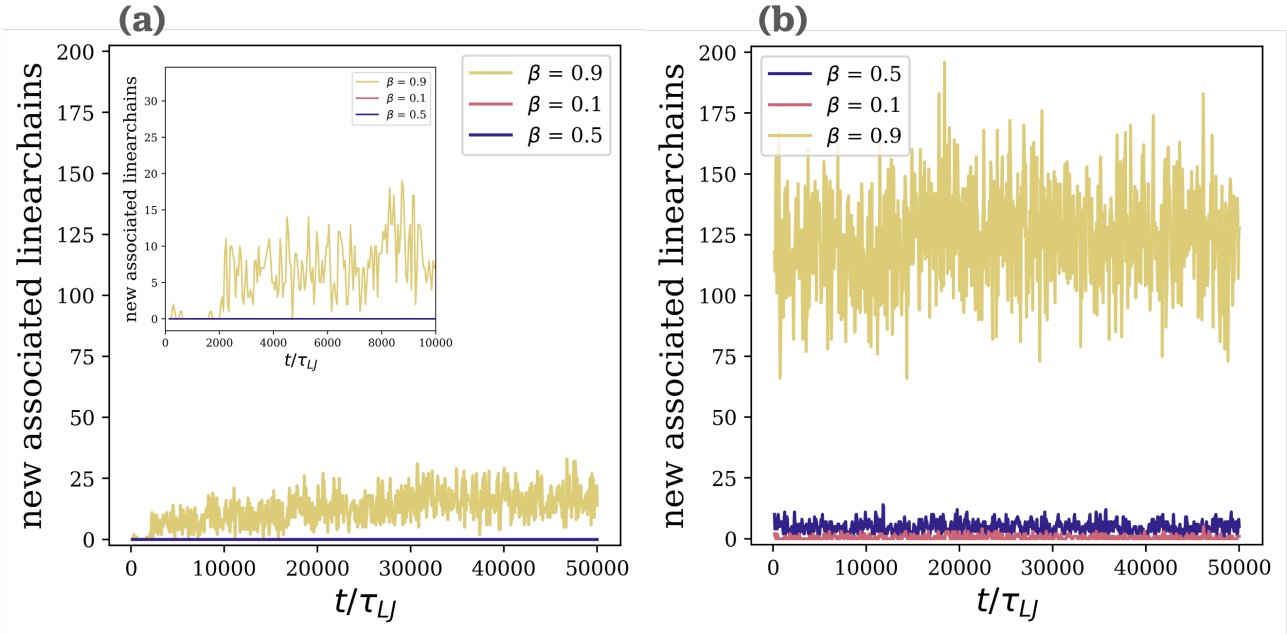

Figure A.4: The changes in the number of LPE for the whole system. (a) dilute regime 0.01 vol%, no exchange of LPEs has been recorded at moderate degrees of neutralization. For high neutralization, no exchange has been initially documented. After 2000 $\tau_L J$, there is an increase in how many LPE are exchanged. Inset is a zoom-in of the start of the production run. (b) overlap regime 1.0 vol%, for low and moderate neutralization there is a minimal exchange, for high neutralization there is a more significant exchange of LPE

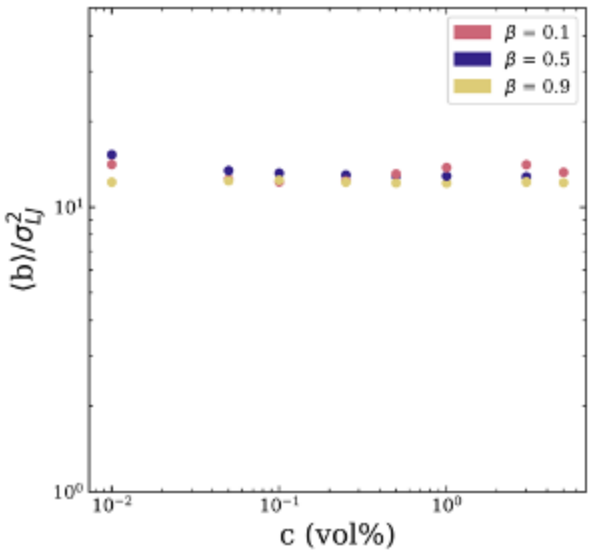

Figure A.5: Average asphericity of the PE-GNPs over the whole ensemble and the whole simulation. This shows the almost concentration-independent asphericity of the PE-GNP.

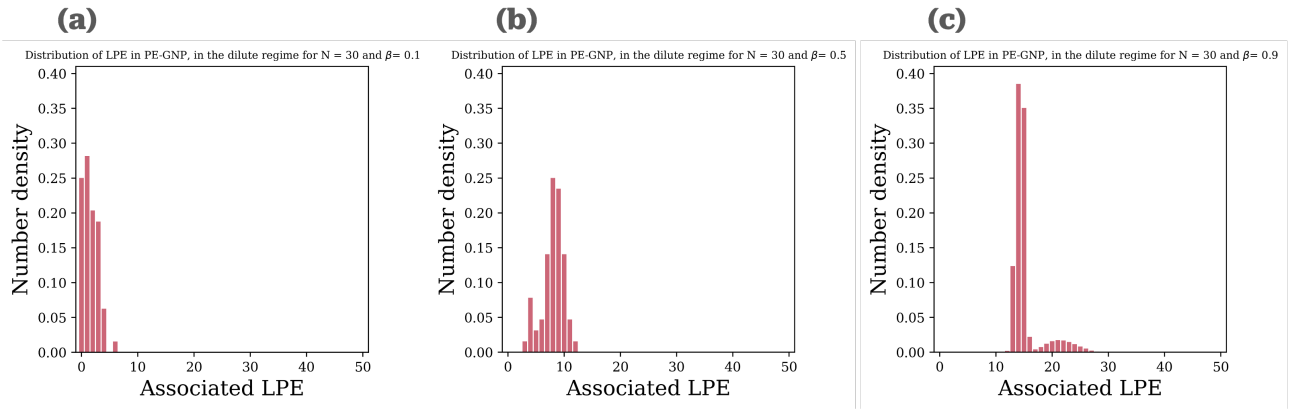

Figure A.6: The distribution of LPE of PE-GNP over the whole simulation, for individual β. An LPE is counted as associated if one of the beads is inside a sphere with an approximated radius from the R_g and the degree of neutralization. dilute regime, 0.01vol%,

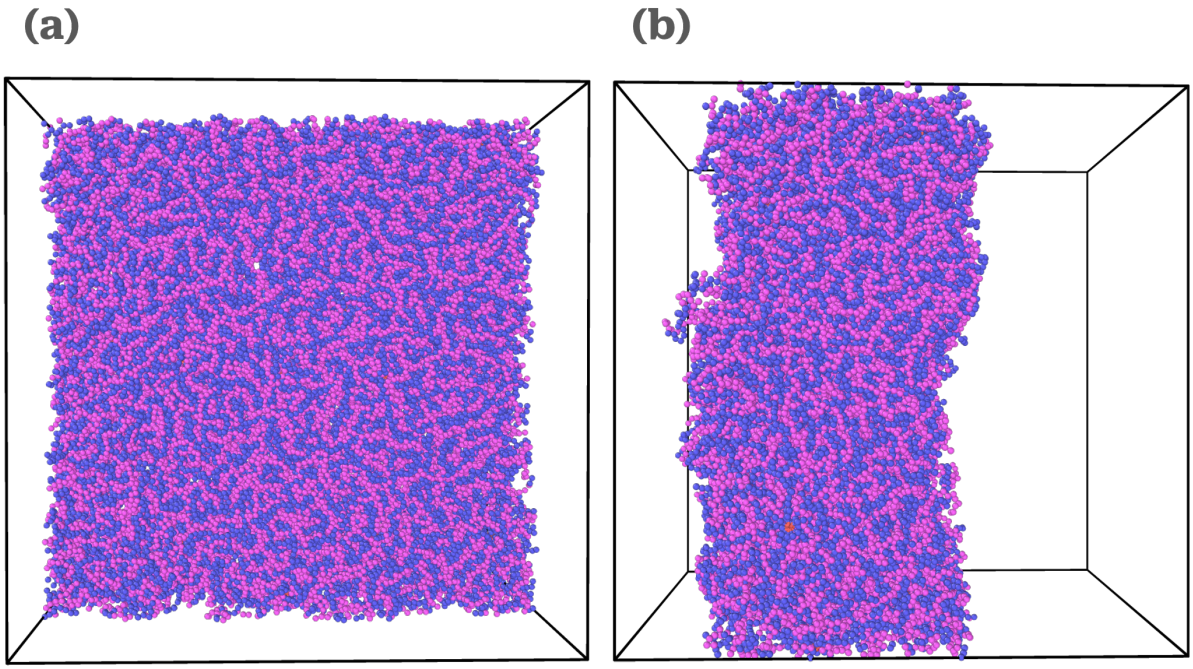

Figure A.7: Simulation snapshots depicting the surface area minimization upon aggregation of all PE-GNP, at $c = 3.0$ vol%, $\beta = 1.0$.

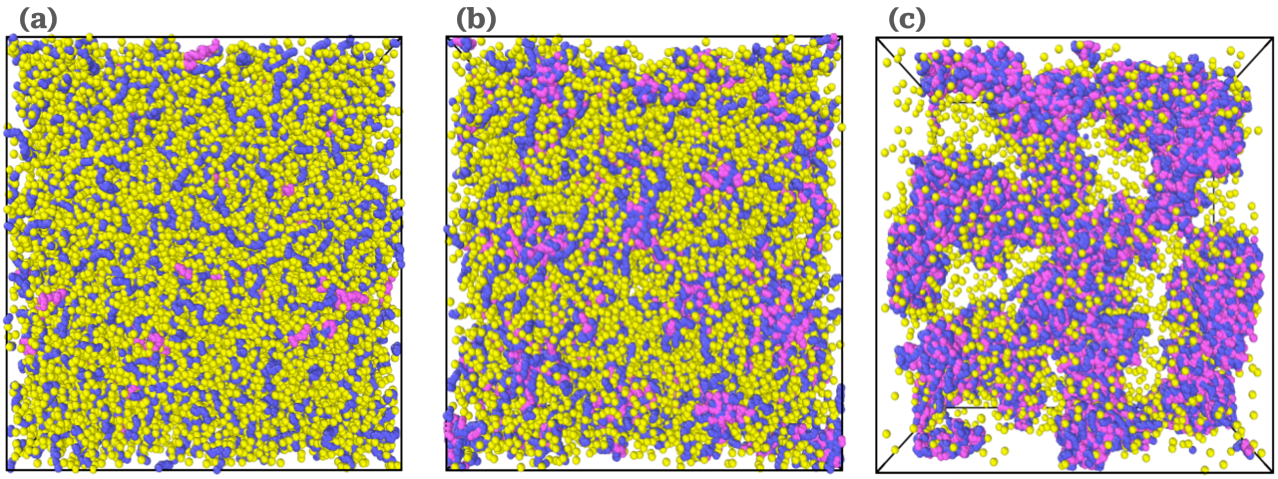

Figure A.8: Simulation snapshots taken with OVITO, constant concentration $c = 1\%$ at different β: (a) $\beta = 0.1$, (b) $\beta = 0.5$, (c) $\beta = 0.9$. Red spheres (not visible) are the cores of the PE-GNPs, blue beads represent the Kuhn segments comprising the arms of the PE-GNPS, and pink beads represent the LPE

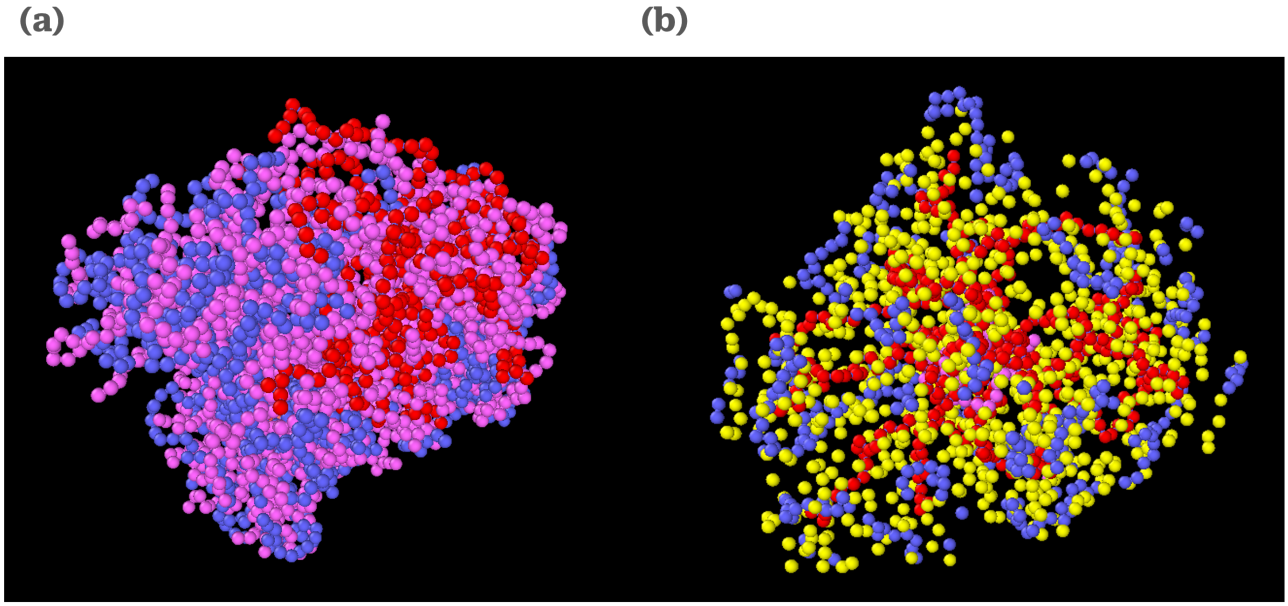

Figure A.9: clariffication of a single GNP in the snapshots used in figure 4.8. (a) showing a dimer complex of two PE-GNPs. (b) shows a PE-GNP surrounded by other PE-GNP and countrions

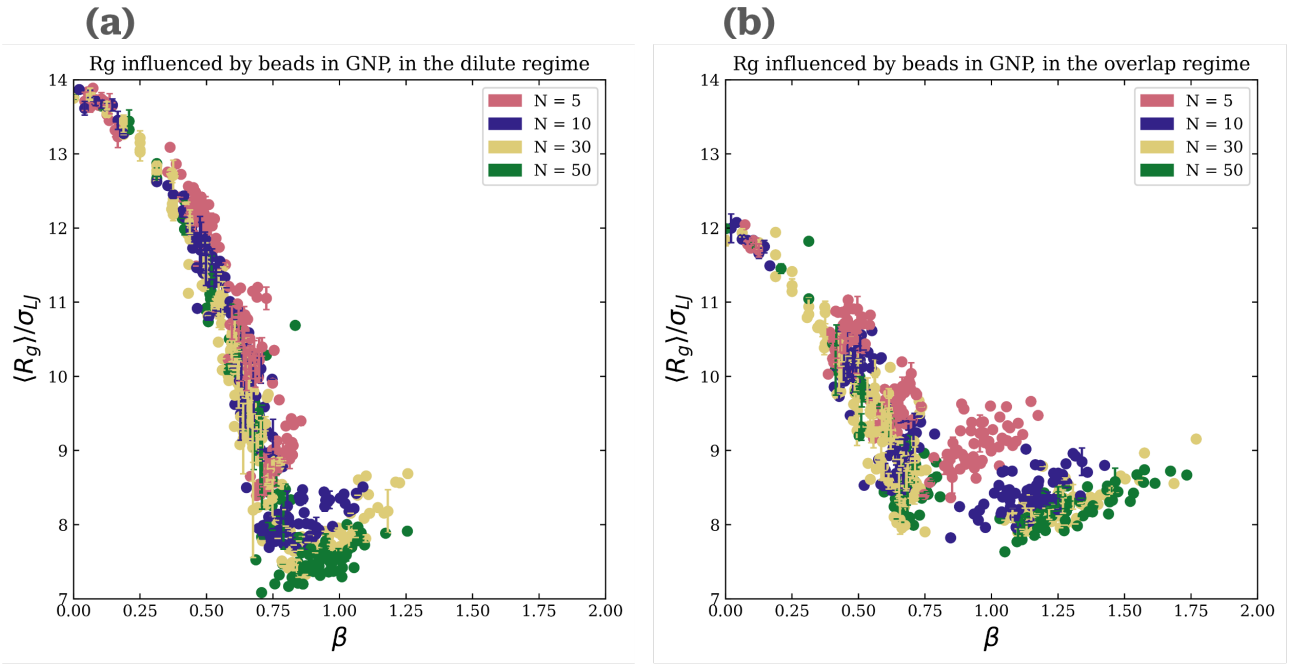

Figure A.10: Individual R_g contributions for different PE-GNP.

A.1 Past complete neutralization

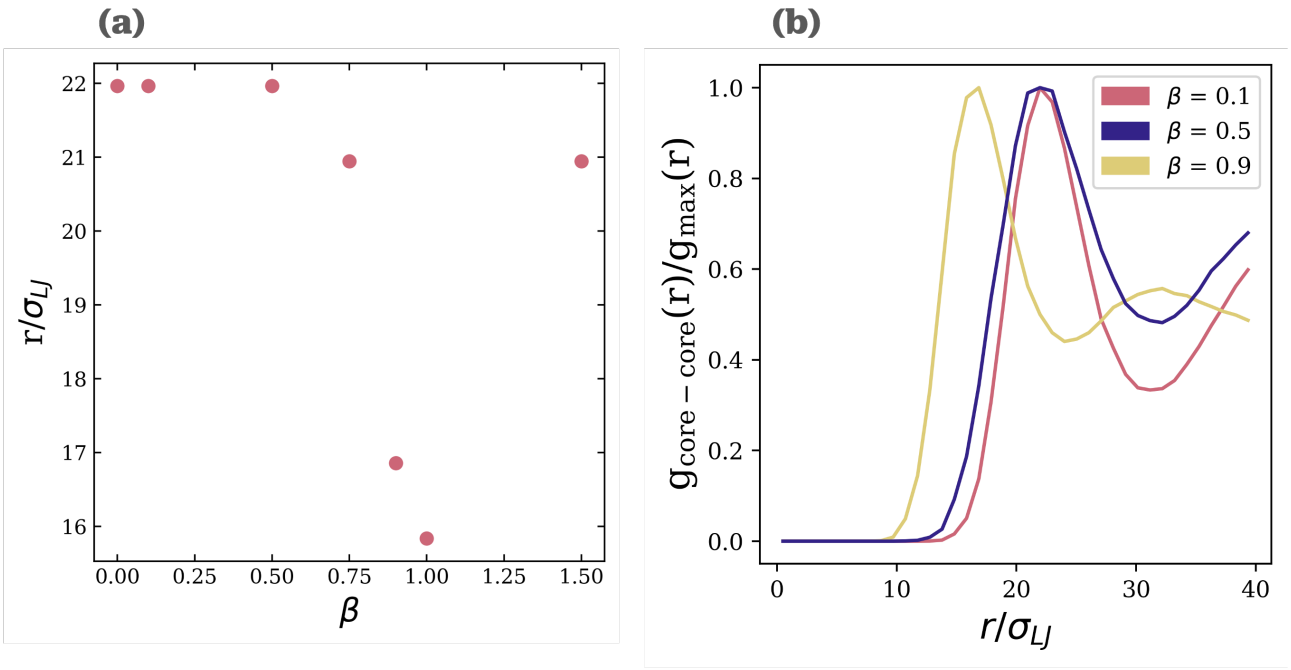

Figure A.11: The figures describe the shrinkage of the inter-core distances at c = 3.0 %. (a) shows the RDF between cores. (b) shows the location on the x axis for the first peak in figure (a) for LPE length N = 30.

Further investigation of the system has shown that upon the addition of more LPE the system becomes a homogeneous phase once more.

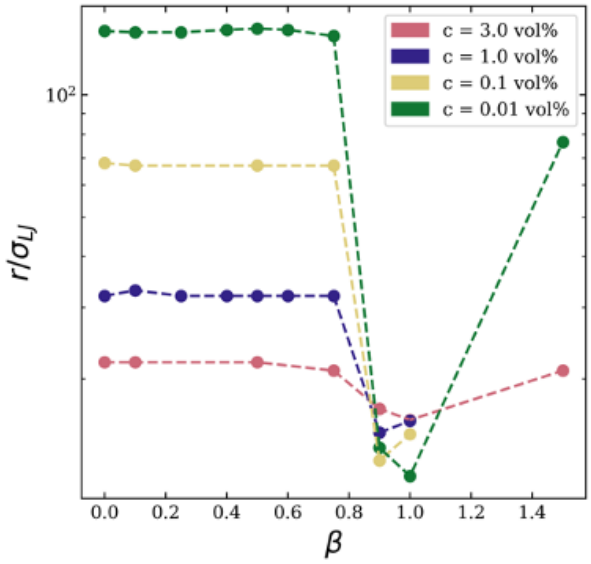

Figure A.12: Concentration dependant collapse or dimerization.

A.2 Dielectric constant

Table A.1: simulation details Dielectric constant (f16-M30), not discussed as of now

Concentrations (vol%)	**dielectric constant,** K
0.01, 0.1, 1.0	0.5, 1, 2, 10
3.0	0.5, 1, 10
0.05, 0.25, 0.5, 5.0	1

The dielectric constant was varied, but no conclusive results were gathered.

B Verification of the simulations

The system was equilibrated to apply the ergodic hypothesis and tested on the end-to-end vector correlation decorrelation of the LPE. The values are reported below.

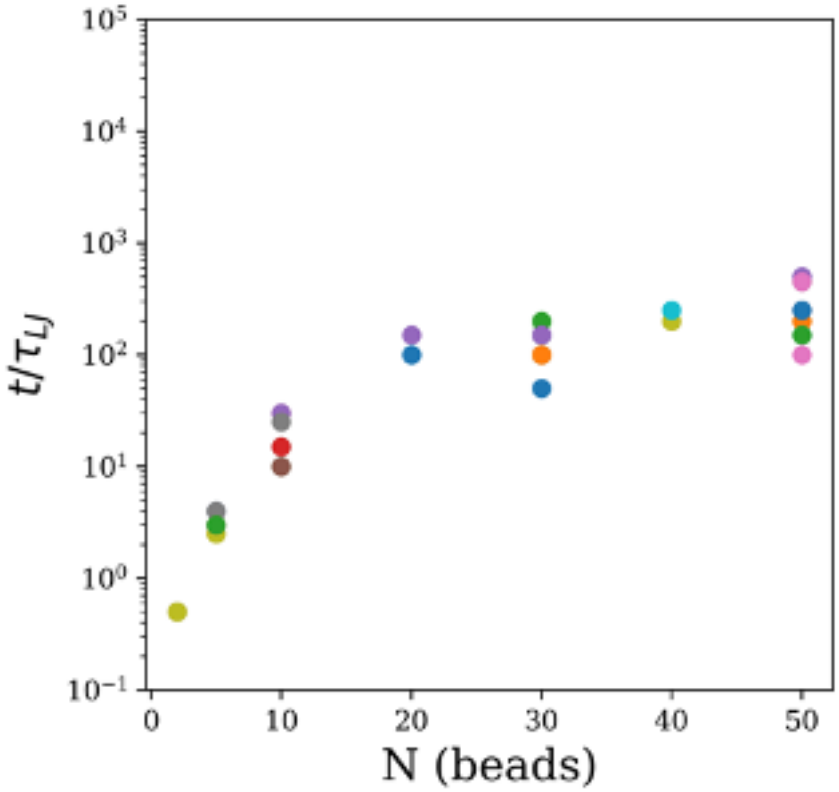

Figure B.1: Relaxation times determined from the correlation decorrelation of the end-to-end vector of LPE

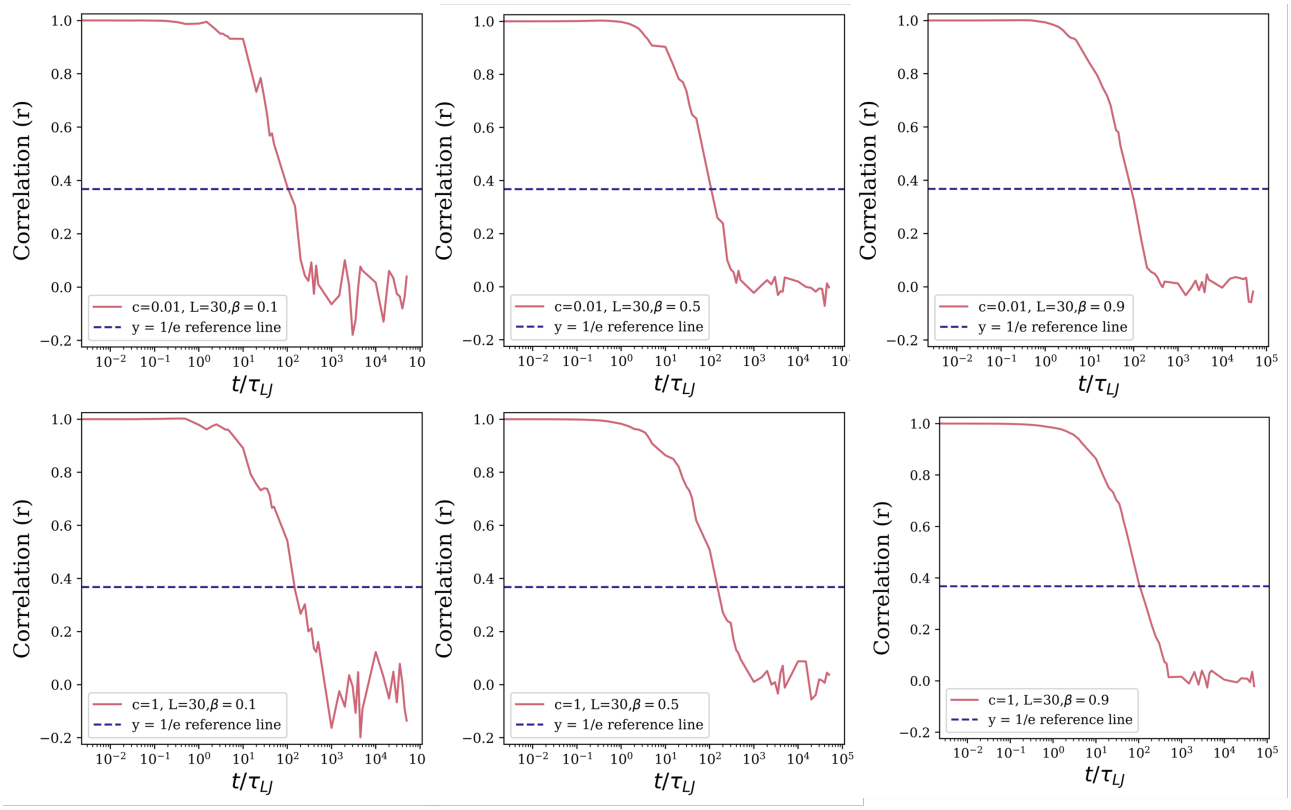

Figure B.2: Examples end-to-end vectors over time. Where the interception with 1/e is taken as the relaxation times for different concentrations and β